Z-mode sounding within propagation "cavities" and other inner magnetospheric regions by the RPI instrument on the IMAGE satellite

D. L. Carpenter,[1] T. F. Bell,[1] U. S. Inan,[1] R. F. Benson,[2] V. S. Sonwalkar,[3] B. W. Reinisch,[4] D. L. Gallagher[5]

Abstract. When the Radio Plasma Imager (RPI) on the IMAGE satellite operates in the inner plasmasphere and at moderate to low altitudes over the poles, regions in which the ratio of the local electron plasma frequency f_{pe} to the local electron gyrofrequency f_{ce} may exceed or be less than unity, pulses emitted at the low end of the RPI 3 kHz to 3 MHz sounding frequency range can propagate in the the Z mode as well as the whistler mode. At medium altitudes within the plasmasphere, discrete echoes with turning points Earthward of IMAGE are often observed, analogous to the regular and oblique Z-mode echoes found on topside sounder records. In the polar regions, where $f_{pe}/f_{ce} < 1$ usually obtains, the echoes tend to be diffuse and to exhibit properties such as an intensity decrease at the local value of f_{ce}, where there is a significant topological change in the Z-mode refractive index surface. At low altitudes near the plasmasphere and in the polar region, passive recordings usually fail to provide clear identification of local plasma parameters, while Z-mode soundings can regularly do so. Within the transition region from the auroral zone to the plasmasphere and the plasmasphere itself, at altitudes from $\approx$ 2000 km upward, we find evidence of the Z-mode cavity phenomenon that has been noted previously in connection with natural wave emissions detected at polar latitudes. Within a Z-mode cavity, discrete Z-mode echoes can be trapped as they propagate along field-aligned paths beween upper-and lower-altitude reflection points. The echoes present unique forms, depending upon whether IMAGE is located above or below a minimum in the altitude profile of the Z-mode cutoff frequency. Through an inversion process, such echoes make possible remote determination of the field-line electron density profile in regions where that profile is poorly known. In two examples, the electron density distribution along the field lines was determined to distances of thousands of km above the location of IMAGE, all on the basis of echo delay information within frequency bands only $\approx$ 30 kHz wide.

1. Introduction

The Radio Plasma Imager (RPI) on the IMAGE satellite was designed to use the classical radio sounding technique at geocentric distances up to $\approx 8\ R_E$ [*Reinisch et al.*, 2000; *Burch*, 2000]. The sounding frequency range was extended downward from 3 MHz to 3 kHz to permit determination of the electron density n_e in outer magnetospheric plasmas as tenuous as $n_e = 0.1cm^{-3}$ and the reception of echoes from remote plasma regions with $10cm^{-3} < n_e < 10^5 cm^{-3}$. In planning the experiments it was realized that signals transmitted at frequencies below the local up-

[1] Space, Telecommunications and Radioscience Laboratory, Stanford University, Stanford, California, USA.
[2] NASA Goddard Space Flight Center, Greenbelt, Maryland, USA.
[3] Department of Electrical Engineering, University of Alaska Fairbanks, Fairbanks, Alaska, USA.
[4] Center for Atmospheric Research, University of Massachusetts, Lowell, Massachusetts, USA.
[5] MASA Marshall Space Flight Center, Huntsville, Alabama, USA.

Paper number .
0148-0227/03/$9.00

per hybrid frequency f_{uh} could propagate in both the Z mode and the whistler mode, these being called "trapped" as opposed to "free space" modes because of the upper frequency limits on their local propagation imposed by the dispersion relations for wave propagation in plasmas [e.g., *Budden*, 1985]. Figures 1a, 1b, and 1c are dispersion diagrams, plots of frequency $f = \omega/2\pi$ versus wave number k that illustrate schematically the relationship between the trapped modes and the "free space" ordinary and extraordinary (O and X) modes used in conventional radio sounding. Figure 1a represents conditions common within and at high altitudes beyond the Earth's plasmasphere, under which the local electron plasma frequency f_{pe} exceeds the local electron gyrofrequency f_{ce}, while Figure 1b represents conditions at low altitudes poleward of the plasmapause, where f_{ce} regularly exceeds f_{pe}. Figure 1c illustrates the intermediate case, when $f_{pe} \approx f_{ce}$.

A key difference between the free space O and X modes and the Z and whistler modes is in the phase velocity, expressed as $2\pi f/k \equiv \omega/k$, which exceeds the speed of light in vacuum for the O and X modes and for the left hand polarized branch of the Z mode at frequencies below the electron plasma frequency f_{pe}, but is subluminous for the whistler mode and the right hand polarized branch of the Z mode at frequencies above f_{pe}. The whistler mode and right hand polarized Z mode are therefore capable of strong resonant interactions with the hot electron plasmas of the magnetosphere. *Sonwalkar*, [1995 and references cited therein] has noted evidence of such interactions in the case of the whistler mode and *Gendrin* [1975], and *Jones* [1977], among others, in the case of the Z-mode.

The operation of a Z-mode/whistler-mode transmitter in the magnetosphere has been an unrealized goal of space scientists for many years. In the late 1970s a NASA study group was formed to consider active wave experiments from the Shuttle [e.g., *Fredricks et al.*, 1978; *Dyson*, 1978; *Inan et al.*, 1981)]. This group and its successor developed plans for a wave injection mission called Waves in Space Plasmas (WISP), to include a transmitter on the Shuttle and signal detection on a sub-satellite. The proposed experiments were to include verification of basic dispersion relations, investigation of coupling between wave modes, and study of wave-particle energy and momentum exchange [*Fredricks et al.*, 1978]. The project was selected for a Shuttle flight in the mid 1980s but was cancelled after the Challenger accident in 1986.

In this paper we discuss Z-mode echoes from RPI that have been detected during routine sounding operations with 3.2 ms pulses and note their potential use in diagnostics of plasma structure. We pay special attention to Z-mode echoing back and forth within trapping regions that may extend thousands of km along field lines within and near the plasmasphere.

An overview of RPI whistler-mode echoes is presented in a paper by *Sonwalkar et al.*, [2003].

2. Instrument description

RPI is a multi-mode instrument [*Reinisch et al.*, 2000] in which sounding and listening frequencies, range detection, pulse characteristics and repetition rate are adjustable parameters over a wide range of values. The instrument covers the frequency range from 3 kHz to 3 MHz with a receiver bandwidth of 300 Hz. There are three orthogonal thin-wire antennas, two 500-m tip-to-tip dipoles in the spin plane (X and Y) and a 20-m tip-to-tip dipole along the spin axis (Z). The long dipoles are used for transmission, and all three antennas are used for reception. The nominal radiated power from RPI, variable (in terms of free space mode excitation) from 0.1 mW at low frequencies to $\approx$ 10 W per dipole at 200 kHz, was

reduced by 3 dB on May 8, 2000 when the power supply for the Y axis transmitter failed. A further reduction occurred on October 3, 2000, when one of the X axis monopoles was partially severed, apparently by a micrometeorite. In spite of these difficulties, excellent data have continued to be acquired, as described below.

3. Observations of Z mode echoes

3.1. Background

In contrast to whistler mode echoes, and by analogy to O-and X-mode echoes, Z-mode echoes are expected to return from locations where a cutoff condition is met, indicated by f_Z in Figures 1a, 1b and 1c. The Z mode is of special interest because, once generated, it may through mode coupling become a source of waves propagating in otherwise forbidden regions, an often cited example being the suggested conversion of upper hybrid waves to O-mode waves in the region near the plasmapause [e.g., *Jones*, 1976]. At the plasma frequency the wavelengths of the O-and Z-mode waves, with wave vector **k** oriented along **B**, are approximately equal and, if the local density gradients are sufficiently large, "tunneling" from one mode to the other should be possible.

Naturally occurring Z-mode waves have been widely observed on satellites such as DE-1, ISIS I and INTERBALL 2, and their spectra have been investigated for information on source mechanisms and propagation [e.g., *Gurnett et al.*, 1983; *Benson et al.*, 1985; *Santolik et al.*, 2001]. For a recent review of auroral Z-mode emissions, see *LaBelle and Treumann*, [2002].

In past ionospheric topside sounding work, Z-mode echoes were regularly observed [e.g., *Hagg et al.*, 1969] thanks in part to their occurrence near 1 MHz at frequencies for which the sounders were designed to operate most efficiently [e.g., *Franklin and MacLean*, 1969]. Z-mode echoes have also been detected during transmissions from ISIS 1 to ISIS 2 in rendezvous situations involving separations of $\approx$ 1000 km or less [*James*, 1979].

Z-mode echoes tend to appear on RPI records whenever X-and O-mode echoes are recorded. The frequency band of allowed Z-mode propagation, however, considered as a fraction of its upper limit f_{uh} (see Figures 1a, 1b, and 1c), varies widely with altitude. At high altitudes within and near the plasmasphere the band shrinks as f_{ce} falls off and the difference between f_{pe} and $f_{uh} = ({f_{pe}}^2 + {f_{ce}}^2)^{1/2}$ diminishes. A similar effect occurs in the topside ionosphere, where the ratio f_{pe}/f_{ce} increases rapidly with decreasing altitude. Thus it is not surprising that most of our reported Z-mode frequency-dependent effects occurred at altitudes between IMAGE perigee at $\approx$ 1200 km and $\approx$ 10,000 km.

We now present evidence of Z-mode echoes obtained by RPI under both the condition $f_{pe}/f_{ce} > 1$ and $f_{pe}/f_{ce} < 1$, as well as evidence of band limited echoing back and forth within regions that act as propagation cavities. In surveying available data, identifying phenomena, and displaying data in the form of range-versus-frequency plots, or plasmagrams, we have employed special software developed by *Galkin et al.* [2000].

3.2. RPI Z mode echoes: condition of $f_{pe}/f_{ce} > 1$

At altitudes in the range $\approx$ 3000–4000 km RPI has detected Z-mode echoes remarkably similar to ones observed in the topside ionosphere, for example by Alouette 2 near 1000 km [e.g. *Hagg et al.*, 1969]. Figure 2a shows a modified ionogram from Alouette 2 [adapted from *Hagg et al.*, 1969]. Echo virtual range (range in R_E assuming free-space speed of light propagation) is plotted versus sounding frequency, with range increasing upward for comparison with the RPI plasmagrams of Figures 2b and 2c. At the time of Figure 2a, on April 6, 1966, Alouette 2 was at 870 km altitude and

at L ≈ 3. The RPI records of Figures 2a and 2b were recorded on July 6, 2001 at ≈ 3100 km and ≈ 4100 km, respectively, with corresponding L values ≈ 2.4 and 2.0. Arrows on both the Alouette and RPI records indicate echoes identified as Z, Z', O, and X, and marks below the records show the approximate values of key plasma parameters at the respective satellite locations.

In the case of Figure 2a, f_{pe} was ≈ 880 kHz, slightly larger than f_{ce} at ≈ 840 kHz. A well defined Z trace begins at f_Z ≈ 550 kHz and extends upward toward a maximum frequency below f_{uh} that is associated with a limit on vertical-incidence propagation [*Jackson*, 1969]. The value of this limiting frequency, ≈ 1.06 MHz in this case, depends not only upon f_{pe} and f_{ce} but also upon the angle between the vertical and the direction of the Earth's magnetic field. In this example, as in the RPI cases below, there were two Z-mode echoes, with the second labeled Z′. In Figure 2a the latter begins at the local f_{pe}, crosses the Z trace and approaches infinite range at the same frequency approached by the Z trace. The Z′ trace was interpreted by *Calvert* [1966] as having propagated obliquely between the satellite and the O-mode reflection level $f = f_{pe}$.

The examples of Figures 2b and 2c were observed 5 min apart as IMAGE moved through the late afternoon lobe of the plasmasphere following perigee. The orbit was roughly similar to the one illustrated in Figure 3b for another case in July 2001 (and discussed below). RPI was transmitting single 3.2 ms pulses at frequency steps of 2 kHz between 350 kHz and 480 kHz. In Figures 2b and 2c, called plasmagrams, virtual range is plotted in R_E and amplitude is color coded in units of dB(nV/m). The minimum observable virtual range is 0.3 R_E because of the 3.2 ms minimum transmitted pulse length and additional time for the receiver preamplifier to recover from the high voltage generated during the transmitter pulses and for the dissipation of stored energy in the antenna coupler.

The echoes marked Z and Z′ and O in Figures 2b and 2c appear to be higher-altitude versions of their counterparts in Figure 2a, and thus appear at sounding frequencies roughly one half those involved in the Alouette 2 data. In the case of Figure 2b, IMAGE was at L ≈ 2.4 and had just entered the plasmasphere. The O and Z′ traces approach zero range at ≈ 358 kHz, and the Z trace extends to the left beyond the low frequency limit of the record. From the satellite ephemeris, f_{ce} ≈ 288 kHz, so that f_{pe}/f_{ce} ≈ 1.24 and the apparent resonance at 460 kHz, located at the upper edge of a diffuse noise band, may be identified as f_{uh}. As in Figure 2a, the Z and Z′ traces cross one another and then approach a maximum frequency, here ≈ 440 kHz, which is slightly lower than f_{uh} ≈ 460 kHz.

In the case of Figure 2c the value of f_{pe} is higher, ≈ 422 kHz, and the value of f_{ce} lower, ≈ 197 kHz, as IMAGE moved farther into the plasmasphere, reaching L ≈ 2.0 and ≈ 4100 km altitude. On this plasmagram f_{uh} is not well defined but is calculated to be ≈ 466 kHz. The echo configurations are similar to those of Figure 2b, but with a characteristic narrowing of the frequency interval between f_{pe} and f_{uh} from ≈ 104 kHz to ≈ 44 kHz as IMAGE moved into a region of larger f_{pe}/f_{ce} (the corresponding interval in Figure 2a is ≈ 320 kHz). During this IMAGE pass, the Z and Z′ traces could be identified on seven successive soundings spaced over 15 minutes. Above an altitude of ≈ 5200 km, as the ratio f_{pe}/f_{ce} approached 4, the Z′ trace could not be resolved due to the limited number of sounding frequency steps (at 2.0 kHz per step) available between f_{pe} and f_{uh}.

It is known from experience with Alouette and ISIS data that a band of noise may be stimulated by a topside sounder between f_{uh} and f_{pe} or f_{ce}, whichever is larger [*Muldrew*, 1969]. Because of the low phase velocities, and hence high Z-mode refractive index in that band (see Figure 1a), the Z-mode waves may undergo scattering in the presence of irregularities, while O-and X-mode waves may not

show such an effect. In this light we interpret the bands of noise at frequencies below f_{uh} in Figures 2b and 2c as sounder stimulated Z-mode noise, although the bands may also include some weak natural Z-mode noise, as in cases from ISIS 2 reported by *Benson* [1993].

3.2.1. Diagnostic potential of the echoes.

During conventional sounding by RPI, the best defined echoes propagate along geomagnetic field aligned paths, but the inversion process for plasma density profiles is often limited to path altitudes above $\approx$ 3000 km because of limits on the high frequency extent of the echoes or problems of accuracy with the echo inversion near the lower altitudes. Because of their comparatively low group velocities, Z-mode echoes may enhance the overall sounding capabilities of RPI in the region below $\approx$ 3000 km. Figures 2b and 2c illustrate differences in travel time between Z and Z′ echoes and O mode echoes when they each represent downward propagation into regions below $\approx$ 3000–4000 km.

3.3. Z-mode echoes: condition of $f_{pe}/f_{ce} < 1$

3.3.1. Observations.

Figures 1b and 1c display the propagation modes when f_{pe} falls below or is approximately equal to f_{ce}, conditions that commonly occur when IMAGE is poleward of the plasmapause and at sufficiently low altitude, where f_{ce} is large. The figures show that in such cases the key frequencies tend to be widely distributed below f_X, the local X-mode cutoff frequency since, for example, f_Z and f_X are separated by the value of f_{ce} unless significant gradients in f_{pe} and f_{ce} are present. Another view of the situation is provided in Figure 4a, adapted from *Gurnett et al.* [1983]. This is a model of the distribution with geocentric radial distance in the polar region of f_{pe}, f_{ce}, f_{uh}, and f_Z, with shading showing the frequency range within which the Z-mode can propagate at a given altitude. On this plot the condition $f_{pe}/f_{ce} < 1$ is shown as prevailing between radial distances of $\approx$ 1.6 R_E and 3.5 R_E. The regions of R-X and L-X polarization (see also Figure 1) are marked, as well as a hatched trapping region where the f_Z curve is double-valued at a given frequency.

Under such conditions plasmagrams may exhibit echo patterns such as the ones illustrated in Figures 5a and 5b, from July 4, 2001 and February 22, 2002, respectively. Here again there are similarities to topside sounder records [e.g., *James*, 1979; *Benson*, 1993] as well as to certain properties of natural emissions observed in the polar regions [e.g., *Gurnett et al.*, 1983; *LaBelle and Treumann*, 2002]. On a scale of virtual range to 4 R_E, Figure 5a shows Z-mode echoes received at $\approx$ 1500 km altitude near perigee at high southern polar latitudes. Amplitude is displayed in dB(nV/m). Single 3.2 ms pulses were transmitted at 66 frequencies spaced by linear 4.0 kHz steps between 600 kHz and 860 kHz. Distinctive features of the record include: (1) diffuse echoes, most with ranges substantially longer than those of order 0.5 R_E to be expected for the O and X modes, (2) echo ranges extending to maximum values that increase with sounding frequency, (3) a gap or weakening of the echoes at an intermediate frequency, and (4) a relatively abrupt upper frequency limit. In this case, the value of f_{uh} at the upper edge of the strong Z-mode activity (see Figure 1b) is $\approx$ 808 kHz. The value of f_{ce} from the ephemeris is $\approx$ 740 kHz, which coincides with the gap in the Z-mode echoes. Thus f_{pe} is calculated to be $\approx$ 324 kHz, so that $f_{pe}/f_{ce} \approx 0.4$.

Figure 5b shows similar echoes on a scale of virtual range to 7.5 R_E and at frequencies from 200 kHz to 1000 kHz, with logarithmic 4% stepping between individual 3.2 ms pulses. In this case IMAGE was at $\approx$ 3440 km altitude and in a transition region between the southern polar ionosphere and the plasmasphere, where the increas-

ing value of local f_{pe} along the orbit tends to become comparable to the decreasing value of f_{ce}. The Z-mode echoes are generally similar to those in Figure 4a but are displaced to lower frequencies, largely because of the lower value of f_{ce}, here estimated from the satellite ephemeris and the gap in the observed echoes to be $\approx$ 378 kHz. At the right, above $\approx$ 480 kHz and at virtual ranges less than $\approx 0.5\ R_E$, are an X-mode echo (arrow) that approaches zero range at a calculated value of $\approx$ 553 kHz. The upper limit of Z-mode propagation at f_{uh} is well defined at 480 kHz, implying that $f_{pe} \approx$ 295 kHz and $f_{pe}/f_{ce} \approx 0.8$.

3.3.2. Interpretive comments.

Figure 4b is an expanded and modified version of the lower part of Figure 4a, qualitatively similar but with a less pronounced falloff with altitude in f_{pe} and thus a correspondingly narrower range of allowed Z-mode frequencies at altitudes of interest. Shown in cartoon fashion are the paths that various Z-mode wave frequencies may follow so as to be received as echoes during an RPI sounding at $\approx$ 4000 km altitude over the southern polar region. The ray paths from RPI are sketched as extending vertically downward from the horizontal line and satellite icon indicating the altitude of IMAGE to reflection at the f_Z cutoff. Frequencies near f_1 exhibit low ranges because of the proximity of the corresponding turning points at f_Z. Within the trapping region, a signal launched upward may in principle be reflected and return, as discussed in a later section, but in the case considered here, well poleward of the plasmasphere, this has not yet been observed.

Frequencies near f_2 tend to exhibit only small variations in group delay with frequency, since increases in mean group velocity along the ray paths compensate for the increasing range to the turning points. Signals emitted between f_3 and f_4 may show an increase in maximum echo delay as well as range spreading of echo delays beginning at minimum range. This behavior is partly attributed to the initial wave-mode conversion at f_{pe} from the slow mode to the fast mode and a corresponding change from right to left polarization (see Figure 1b). As pointed out by *Gurnett et al.* [1983], at f_{pe} there is a complicated change with frequency in the refractive index surface near zero wave normal angle, from a nipple above f_{pe} to a dimple below f_{pe} [*Budden*, 1961]. In a study of Z-mode echoes on Alouette 2 ionograms, *Colin and Chan*, [1969] pointed out that for small wave normal angles, as may be the case for downward propagation at polar latitudes, the group refractive index for Z-mode propagation develops a peak at f_{pe} whose sharpness increases with the value of f_{ce}/f_{pe}.

Signals emitted near f_5, between f_{ce} and f_{uh}, must (for the ray paths illustrated) pass the f_{pe} level twice, and must initially cross the level where f = f_{ce}. It is apparently the inhibition of this crossing that underlies the clear break in the Z-mode echoes shown in Figure 5. The effect may be partially understood in terms of the variations in Z-mode propagation at f_{ce} pointed out by *Gurnett et al.*, [1983] in their discussion of natural Z-mode emissions observed in the auroral region on DE-1. As a sounder steps in frequency from below to above the local value of f_{ce}, the refractive index surface evolves from an elongated (along **B**) cigar shape to a resonance-cone type of surface in which a range of angles near the **B** field direction is forbidden. If the electron density gradients are along the magnetic field direction, Z-mode waves propagating at frequencies above f_{ce} are not expected to cross the f_{ce} level, but in the case of gradients perpendicular to **B**, *Gurnett et al.* point out that such crossings should occur smoothly. In the polar regions, field aligned density structures are known to be regularly present, so that crossing of the f_{ce} level by higher frequency echoes should regularly occur but may be inefficient. As the sounding frequency approaches f_{uh}, the signals become increasingly quasi electrostatic, giving rise to

the possibility of strong interactions with irregularities and a wide spread in echo delays.

3.3.3. Diagnostic potential.

RPI operates as a sweep-frequency receiver at intervals between soundings so as to provide information on local plasma parameters and natural noise phenomena [e.g. *Reinisch et al.*, 2001a; *Benson et al.*, 2003]. During low altitude passes over the polar regions, however, the plasma density may not be readily determinable by this means because the local value of the UHR increases to a peak that is dominated by f_{ce} and tends to be poorly defined in the passive RPI data. In contrast, f_{uhr} as well as f_{ce} are often well defined when the sounder is operated, as illustrated in Figures 5a and 5b, so that the local value of f_{pe} may be obtained.

3.4. Echoing within a Z mode trapping region

3.4.1. Introduction.

A remarkable feature of Z mode echoes from RPI is the occurrence of echoing back and forth within a localized trough-like depression in the profile of f_Z with altitude. Such depressions are indicated in Figures 4a and 4b. As noted above, they are called trapping regions because waves propagating at frequencies that are above f_Z at the satellite but below the peak value of f_Z at the upper "edge" of the trough are in principle confined to the trough region.

Because the observed echoes appear to undergo multiple hops back and forth between echo points in widely different directions from the spacecraft, we suggest that they are guided along geomagnetic field-aligned irregularities in a manner analogous to that of X-and O-mode echoes that return to IMAGE from regions on opposite sides of the magnetic equator [e.g. *Reinisch et al.*, 2001b].

The existence of a trough in a limited altitude region can be qualitatively understood by considering the dependence of f_Z on f_{ce} and f_{pe}/f_{ce}, namely: $f_Z = (f_{ce}/2)[-1 + (1 + 4(f_{pe}/f_{ce})^2)^{1/2}]$. At most altitudes of interest f_{ce} varies monotonically with distance along the geomagnetic field, while f_{pe}/f_{ce} at first decreases from values of order 5 near the peak of the ionosphere, reaching minimum values (in some cases < 1) at altitudes of several thousand km, where the light ions begin to dominate the altitude profile. Above this region the ratio tends to increase because of the large scale heights of the light ions. Depending upon the form of the f_{pe}/f_{ce} profile near its minimum values, the corresponding f_Z profile may exhibit a minimum, and hence a trapping region, as illustrated in Figure 4.

Z-mode trapping effects are found both within the plasmasphere and in the plasmapause region, and to occur both when $f_{pe}/f_{ce} > 1$ and when $f_{pe}/f_{ce} < 1$. At least two distinctive plasmagram echo forms have been observed, apparently depending upon whether the sounder is located above or below a minimum in f_Z, i.e., whether the local gradient of f_Z along the field line is positive or negative.

3.4.2. Trapping effects detected at altitudes below a Z-mode trough minimum.

Examples of Z-mode trough echoing detected at an altitude below a trough minimum (i.e., where $d(f_Z)/ds$ is negative) are shown in Figures 6a and 6b, which display virtual range to 4.1 R_E versus frequency from 180 kHz to 245 kHz. In the case of Figure 6a, from July 26, 2001 and $\approx$ 1700 MLT, IMAGE was at L $\approx$ 3.2 and $\approx$ 3800 km altitude following perigee. As shown schematically on the orbit plot of Figure 3a, the satellite was moving through the region of density gradients from the southern polar region into the plasmasphere. There are four main echo groups, all beginning at a lower cutoff frequency of $\approx$ 194 kHz. Two of the echo forms are similar in appearance to the "epsilon"-shaped echoes observed when RPI X-mode signals are found to propagate along field line paths to reflections points in both hemispheres [e.g., *Fung et al.*, 2003]. At the lower edge of the record there is an echo that rises

from an apparent zero range cutoff near 194 kHz and then exhibits a virtual range near 0.4 R_E at frequencies extending to the upper limit of the record. Above, beginning near a range of 1.4 R_E, is an echo with three strong elements that rise in frequency from a sharp lower limit of $\approx$ 194 kHz. A second and similar triplet echo begins at $\approx$ 2.8 R_E, and the lower part of a third (cut off by the range limit of the sounding program) begins not far below 4.2 R_E. To the right in Figure 6a are some weak looping or rising echoes whose nature is not yet known.

In the case of Figure 6a we find that the echoes began at the local Z-mode cutoff f_Z and that the propagation-mode distributions were as depicted in Figure 1b, with $f_{pe}/f_{ce} \approx 0.9$ at the IMAGE location. From the cutoff frequency 194 kHz and a model value of f_{ce}, 382 kHz, we find f_{pe} to have been $\approx$ 334 kHz. This density value is consistent with results from other orbits in the same region for which information on the plasma parameters could be derived from the sounder data on plasma resonances.

Figure 6b shows an example of a similar Z-mode echoing event recorded 14 days earlier on July 12, 2001. In this case the rising elements are more diffuse, suggesting an influence of fine density structure within the principal guiding channels. Once again, IMAGE was outbound from perigee and in the transition region from the polar cap to the plasmasphere at L $\approx$ 2.9 and 2700 km altitude. From the clear Z-mode cutoff at 216 kHz and the value of $f_{ce} \approx$ 469 kHz (known from a model and from an RPI sounding 30 seconds later at higher Z-mode frequencies), f_{pe} was found to be $\approx$ 384 kHz. Thus $f_{pe}/f_{ce} \approx 0.8$, close to the value for Figure 6a.

In this case there was clear evidence of both the whistler mode and the L-X Z mode. Weak whistler mode echoes (marked "W") appear at the left at a virtual range of $\approx$ 1.15 R_E, and continue at low levels and at roughly the same virtual range to the upper frequency limit of the record. Similar examples are discussed in a companion paper on RPI whistler-mode echoes by *Sonwalkar et al.* [2003].

3.4.3. Interpretive comments on the epsilon-shaped events.

In Figure 6a, the ranges of the echoes near 1.5 R_E are clearly too short to be explained by field-aligned propagation to the conjugate hemisphere, for which virtual ranges of at least 4 R_E would be required (see Figure 3a). Instead, they may be understood as the result of echoing back and forth within a trough in f_Z such as the one in the lower left panel in Figure 4.

Figure 7a shows an interpretive tracing of the Z-mode echoes in Figure 6a with labels representing the combinations of propagation along a "short" path A and a "long" path B that the echoes are believed to represent. Above $\approx$ 198 kHz, the range corresponding to a single traversal of path A (bottom of the record) remained at $\approx$ 0.4 R_E over all the documented frequencies. Meanwhile the bottom element in the first rising echo group shows the result of a single traversal of path B. The second and third elements in this group have ranges A+B and 2A+B. In the next group of three echoes the first element corresponds to the shortest possible path combination, A+2B (a 2B path is not possible except at the local f_Z), the second to 2A+2B, and the third to 3A+2B . Thus within each group of three elements the neighboring echoes are separated by $\approx$ 0.4 R_E, the virtual range of short path A.

The locations of the various paths are sketched in Figure 7b, which displays an idealized profile of f_Z in coordinates of distance along a field line from IMAGE versus frequency, in the manner of Figure 4 but with distance plotted upward. We assume that at the time of Figure 6a, IMAGE was located along the low-altitude side of the f_Z minimum, as shown in the figure. At any transmitted frequency, path A extends from IMAGE to lower altitudes, path B to higher altitudes.

Consider three sounder frequencies, f_1, f_2, and f_3, with f_1 at

the approximate value of f_Z at the IMAGE location. When the stepping sounder frequency reached f_1, only an upward propagating wave was launched, along path B (no excitation of a path A). This wave was reflected at the altitude where f_Z, after passing through a minimum, equaled its value at the IMAGE location. After returning to IMAGE and a local reflection, the wave continued to propagate back and forth along path B, forming the nose-like low-frequency beginnings of the echoes in Figures 6a and 7a. Thus these beginnings appear to be centered at multiples of the path B range for f_1.

Sounder frequencies f_2 and f_3 were both above the local f_Z. At f_2, downward propagation on path A was possible, and waves returning along both paths A and B could act as sources for continued propagation and reflection. At f_3, only path A was available for echoing.

According to Figure 1b, the group velocity of the Z mode should rise with frequency at frequencies not far above local f_Z, and one might therefore expect the elements in the main echo groups to fall in virtual range with frequency rather than to rise as shown in Figure 5a. There are indications that within a few kHz above the cutoff, from $\approx$ 194 kHz to $\approx$ 198 kHz, the echo ranges on path B do in fact decrease. We suggest that above that frequency, however, because of the comparatively gradual increase in f_Z with altitude above the trough minimum, increases in distance to the echo turning point more than compensated for the effects of increasing group velocity. This view is supported by calculations reported in a later section.

If the f_Z altitude profile in Figure 7b were symmetrical about its minimum, the A component might have been expected to show an increase with frequency rather than a nearly constant level. We suggest that below the spacecraft, the f_Z curve rose relatively steeply in such a way as to balance increasing group velocity with increasing distance to echo turning points.

3.4.4. Trapping effects detected above a Z-mode trough minimum.

When IMAGE is located within a Z-mode trapping region but above the trough minimum (i.e., where $d(f_Z)/ds$ is positive) the echo pattern observed is quite different from the one just described. Figures 8a and 8b show 350 – 480 kHz plasmagram examples from successive soundings $\approx$ 1500 km apart on July 28, 2001. IMAGE was moving outbound and upward through the plasmasphere at $\approx$ 1700 MLT, as illustrated on the orbit plot of Figure 3b. The record of 8a was obtained at $\approx$ 4000 km altitude and at L $\approx$ 2.3, where f_{ce} was $\approx$ 280 kHz (from the IMAGE ephemeris) and f_{pe} was $\approx$ 492 kHz (from a combination of f_{ce} and observed f_Z), so that $f_{pe}/f_{ce} \approx$1.8. The data of 8b were recorded 2 1/2 min later at $\approx$ 4500 km altitude and L $\approx$ 2.1, where f_{ce} was $\approx$ 221 kHz (note the $2f_{ce}$ resonance at 442 kHz) and f_{pe} was $\approx$ 515 kHz (again from observed f_Z), and thus $f_{pe}/f_{ce} \approx$2.3.

In both Figures 8a and 8b, there are several discrete echoes that increase in virtual range with frequency, as well as one that curves downward and then extends to higher frequencies near a virtual range of 1.0 R_E. The overall echo patterns on the two plasmagrams are similar. Note in Figure 8b a $2f_{ce}$ gyroresonance at 442 kHz.

Figure 9 is similar in form to Figure 7, containing an interpretive tracing of the discrete elements in Figure 8a and an interpretive path sketch similar to that of Figure 7b. Once again we use three frequencies f_1, f_2, and f_3. IMAGE is assumed to be located at an altitude above the minimum in f_Z. Propagation paths extending downward (Earthward) from IMAGE are labelled C, and paths extending upward D.

At f_1, the value of f_Z at the IMAGE location, the C component is detached from the baseline, as in the case of the B component in Figure 7b. The range is near 2.0 R_E in the case of Figure 8a and near 2.5 R_E in Figure 8b. In Figure 8a a part of 2C may also be seen

at the top of the record. The beginning of a D path at zero range may also be seen in both figures.

At frequency f_2, both C and D paths are detected, and path combinations C+D and 2C +D (D+C+D) are now observed. Echo D rises rapidly in range as an apparent upper frequency limit is approached. In Figure 8a this upper limit is near 405 kHz, about 32 kHz above the local f_Z, while in Figure 8b it is near 437 kHz, only about 18 kHz above f_Z.

Frequency f_3 is above the range of the trapping region, and as a result only path C yields an echo. In both Figures 8a and 8b echo C extends beyond the apparent frequency limits of echo D, with a particularly large extension in Figure 8b.

As noted above, a key to the existence of a Z-mode cavity is the occurrence of a minimum in f_{pe}/f_{ce} with distance along **B**. However, it is not necessary that the ratio f_{pe}/f_{ce} fall below 1, at least at the sounder location, as it does in the situation of Figure 4b. This is indicated by our finding of cavity effects in the plasmasphere during soundings at locations where $f_{pe} \approx 500$ kHz and $f_{pe}/f_{ce} \approx 2$. That such cavities were less "deep" than those detected in the region of plasmapause gradients (Figures 6 and 7) is suggested by comparing ratios of upgoing signal frequency spread to the value of f_Z at the sounder ("spread" meaning in Figure 7 or Figure 9 the difference in frequency between f_1 and the highest frequency echoes returned from upgoing f_2. In typical cases of sounding below the cavity minimum and in the plasmapause region, where $f_{pe}/f_{ce} < 1$, we found the frequency spread to be 35 to 40 kHz, with $f_Z \approx 200$ kHz. In contrast, in the plasmasphere cases, in which $f_{pe}/f_{ce} > 1$, the frequency spread was 10 to 25 kHz, with $f_Z \approx 400$ kHz. This factor of ≈ 4 difference in cavity "depth" is at best only a crude measure of the f_Z field line profiles. A global mapping of cavity profiles is to be desired, but is beyond the scope of the present paper.

3.4.5. A trapping region event detected at 9300 km.

The trapping region events shown above were detected below 5000 km altitude, but such events are not limited to that region. Figure 10 shows portions of a plasmagram from May 14, 2002, with an echo form similar to those of Figures 8a and 8b, but from an altitude of about 9300 km and at L ≈ 4 near 0930 MLT. IMAGE was moving inbound toward the plasmasphere within a region of plasmapause-associated density gradients. The discrete echo components exhibit the same path combinations noted in Figures 8a and 8b, although in this case the frequency stepping was not linear as in Figure 8 but logarithmic 4% over a wider range.

In Figure 10 the C echo at the local f_Z cutoff, ≈ 63 kHz, may be seen near 2.5 R_E. A 2C component (not shown) was also found with range near 5.0 R_E. Note the location of the upper hybrid resonance at ≈ 137 kHz and the presence at the lower right of a weak X-mode component with cutoff close to the expected value (from f_Z and f_{ce}) of 156 kHz. A difference from the cases above is the U-shaped loop formed by echo component C. This type of echo form has been observed on many records, but has not yet been analyzed in detail. The rising part of echo C near 100 kHz occurs near the local values of f_{ce} and f_{pe}, which are ≈ 93 kHz and ≈ 98 kHz, respectively. This additional delay, commonly observed by the ISIS sounders [e.g., *James*, 1979; *Benson*, 1993], may be associated with the peak at f_{pe} in the Z-mode group refractive index for small propagation angles noted by *Colin and Chan*, 1969.

3.4.6. Non-trapped echoes generated within a trapping region.

Figures 11a and 11b show plasmagrams of echoing within a trapping region accompanied by a "normal" Z-mode echo beginning at the local f_Z. Both cases, from July 23, 2001, involve trapped echo forms that we associate with a spacecraft position above a minimum in the f_Z altitude profile. The data of Figure 11a were recorded at $\approx$

5500 km altitude and at L ≈ 2.4 within the plasmasphere at ≈ 1700 MLT, and those of Figure 11b, also within the plasmasphere, at ≈ 3900 km altitude and L ≈ 2.3. In both cases the region of steeper plasmapause gradients was roughly 1000 km from IMAGE.

In Figure 11a the various C and D components (see Figures 8 and 9a) are evident, although the frequency band from the f_Z cutoff of 410 kHz to the upper limit of the D trace is only ≈ 14 kHz in width. The additional element of interest is the trace extending from essentially zero range near the f_Z cutoff to ranges near 0.5 R_E at the upper limit of the record. In this case f_{pe} was ≈ 498 kHz and f_{ce} ≈ 196 kHz (a second harmonic of f_{ce} at 394 kHz is marked on the record).

In Figure 11b, the activity at and just above f_Z was below the frequency range of the record, but the descending loop of the C component is well defined as it merges with what appears to be a normal, non-trapped, echo that rises in range with frequency. Both appear to curve upward in range as they approach the plasma frequency, which we associate with the strong vertical trace at 460 kHz. This is supported by a well defined determination of f_X at ≈ 640 kHz roughly 20 seconds later as well as a value of f_{ce} ≈ 310 kHz from the ephemeris data.

3.4.7. The possibility of launching both direct and trapped echoes.

The direct echoes beginning at or near zero range in Figures 11a and 11b would appear inconsistent with the occurrence in both cases of echoes that reflected from the low altitude boundary of a Z-mode trough (as in the case of the C component in Figure 9) and which were clearly detached from the zero range base line. The frequency coverage of the observed direct signals is as wide or wider than that of the downward launched detached (C-path) echoes (see also Figure 12c), suggesting that reflections of the former took place along ray paths extending generally earthward of IMAGE. We speculate that while the f_Z profile below IMAGE in the field line direction contained a minimum, possibly a quite shallow one, the profile in some other direction, more nearly vertically downward and inward, did not, thus allowing for initial reflections close to IMAGE. Note that in Figure 11b the two types of down-going signals converged in range as the sounding frequency approached f_{pe}.

3.4.8. Examples from apparent crossing of a Z-trough minimum.

Figure 12 shows plasmagrams from a sequence of three soundings on July 13, 2001 as IMAGE moved through a region of increasing electron density in the low altitude plasmasphere. An inset at the right shows the approximate location of the soundings along the IMAGE orbit. The inner edge of the plasmapause is shown to be at L=4, as determined from passive electron density measurements during exit from the late afternoon plasma lobe. In Figure 12a the echoes follow the pattern of Figure 6 that we associate with an IMAGE location below an f_Z trough minimum. The local f_Z was ≈ 229 kHz, and the other plasma parameters were similar to those found for the cases of Figure 6, with f_{ce} ≈ 388 kHz and f_{pe} ≈ 376 kHz. In Figure 12b, recorded 3 min later, at least two echoes rise in range with frequency (one partially obscured at the left). Diffuse echoes at ranges $< 1R_E$ are present over a wide range of frequencies, suggesting reflection from an irregular region below IMAGE. At this time, we infer that IMAGE was near an f_Z trough minimum. We tentatively interpret the rising traces as echoes returning from the high altitude side of the trough, possibly excited at multiple values of local f_Z because of synchronism between the sounder frequency and changes in f_Z along the orbit.

In Figure 12c, after another 2 1/2 min, an echo pattern similar to that of Figure 8 appeared. IMAGE had apparently moved to a position from which a downward propagating C component (Figure

9b) could be excited, with $f_{ce} \approx 240$ kHz and $f_{pe} \approx 523$ kHz. Note also that a direct downward component is present, as in the cases of Figure 11.

The trough effect clearly persisted as the local ratio of f_{pe}/f_{ce} increased from ≈ 1 to 2.2 while the IMAGE altitude increased by only $\approx$ 1100 km. This persistence is consistent with the idea that the f_Z trapping region is an essentially ubiquitous phenomenon, albeit variously shallow, because of the occurrence of an altitude minimum in f_{pe}/f_{ce}, and not its value at the minimum.

3.4.9. Notes on occurrence of trapped Z-mode echoes.

A visual survey was made of plasmagrams from 56 IMAGE orbits in the period June 28–July 31, 2001. There were 112 low altitude crossings of the plasmapause, during half of which one or more signatures of echo trapping were observed. Echoes from satellite locations below the f_Z trough minimum were found on 45 soundings performed at altitudes of $\approx$ 2500–4000 km. In 21 of those cases, the echoes closely resembled the data of Figure 6, while in another 24 the epsilon form was evident but there were complexities such as short precursors before the main epsilon or compression of the entire event into a single band of frequencies of order 5 kHz in width. In all cases the events occurred in the transition region between the plasmasphere and the polar region, at locations where $f_{pe}/f_{ce} < 1$ but near locations where the curves of f_{pe} and f_{ce} along IMAGE orbits cross one another. The electron density was usually a factor of ≈ 2 lower than at nearby plasmasphere locations along the orbit. In all but one case only a single event was seen during a plasmapause crossing.

Trapped echoes from locations above trough minima were seen on 30 soundings performed at altitudes above $\approx$ 3500 km. In 14 of these the echoes were essentially identical in form to those in Figure 8, while in the other 16 the signature was incomplete, tending to show echoes from downward or upward directions only. All but one of the cases occurred within the plasmasphere and, in general, the condition $f_{pe}/f_{ce} > 1$ prevailed. In a number of cases, as illustrated in Figure 8, two events were observed in succession, 2 1/2 minutes apart.

We conclude that in the 34 days studied, the conditions for trapped echoes, including a cavity in the Z-mode altitude profile and field aligned guidance by irregularities, were present at essentially all times. Lack of echoes from below trough minima on some crossings is attributed to unfavorable timing of the 180–245 kHz soundings. Such soundings occurred only for $\approx$ 20 sec every 2 1/2 minutes, and the time that IMAGE typically spent in the region of plasmapause gradients was $\approx$ 2 minutes. Lack of echoes from above trough minima on some orbits is attributed to a combination of spatial variations in the form of the f_Z trough profiles as well as sounding duty cycle limitations.

4. The diagnostic use of trapped Z-mode echoes

4.0.10. The inversion method.

The Z mode as observed in RPI soundings at medium altitudes offers a new tool for studying the distribution of plasma along field lines above the regular ionosphere, both in the region of plasmapause gradients and in the main plasmasphere. An inversion method to accomplish this task is described in the appendix. Below we present the results of the inversion process applied to three examples.

4.0.11. Results of the inversion.

Figure 13 shows the results of the inversion technique applied to the two upward propagating Z-mode signal traces shown in Figures 8a and 8b. In each figure it is the same trace as that labelled 'D' in Figure 9. Figure 13 shows the cold electron density as a function of magnetic latitude for the two traces. The data of Figure 8a were

acquired at L $\sim$ 2.3 at an initial magnetic latitude of $\sim 33^\circ$. The data shown in Figure 8b were acquired at L $\sim$ 2.1 at an initial magnetic latitude of $\sim 26^\circ$. The associated electron density plots are labelled by L shell.

Figure 13 also contains a third curve shown by dashed lines. This curve was plotted with the aid of an empirical model constructed by *Huang et al.* [2003] from RPI data acquired on June 8, 2001. *Huang et al.* [2003] used a different inversion method from that described herein in conjunction with different wave modes and echo data from multiple field line propagation paths to develop their cold plasma density model for the plasmasphere. The dashed curve represents 80 % of the actual value predicted by the *Huang et al.* [2003] model for the L=2.3 magnetic field line. We have scaled down the curve in order to show how well the form of the two curves for L=2.3 agree. At these L shells, variations in cold electron density of 20 to 30 percent with time, longitude, and magnetic disturbance activity are common [e.g., *Carpenter and Anderson*, 1992].

The L=2.3 curve shown in the figure covers a distance that extends to $\sim$ 5000 km above the IMAGE spacecraft. It is remarkable that while the Z-mode virtual ranges in Figures 8a and 8b are only well defined over a range of about 30 kHz above the local value of f_Z, they still provide information on f_{pe} out to a large distance above the spacecraft.

Figure 14 shows the results of the inversion technique applied to the upward propagating Z-mode signal trace of Figure 6a, which is the same as the trace labelled 'B' in Figure 7a. This type of signal trace is produced when the spacecraft is located below the altitude of the minimum in the f_Z profile, as illustrated in Figure 7b. All curves in the figure show cold plasma density as a function of magnetic latitude, λ_m. The portion of the solid curve at the bottom of the figure for $13^\circ \leq \lambda_m \leq 44^\circ$ represents the plasma density as derived from the virtual range information in Figure 6a. The remainder of the curve is an extrapolation of the derived portion to the magnetic equator. The upper solid curve represents the predictions of the *Huang et al.* [2003] model for L=3.2. The dashed curve represents the upper curve scaled down by the factor 0.7 in order to show the close correspondence between the shapes of the two curves. The lower densities derived from the Z-mode data are consistent with the movement of IMAGE through a region of plasmapause density gradients at the time of the measurements.

On the basis of the analysis in the appendix, we find that in all of the cases discussed above, the value of the plasma frequency as a function of distance s along B_o above the spacecraft location can be obtained to a reasonable approximation from the relation:

$$f_{pe}(s)^2 = f_{Zl} f_{ce}(s) + f_{Zl}^2,$$

where f_{Zl} is the value of f_Z at the sounder location. For the July 2001 RPI data and IMAGE locations below an f_Z trough minimum, the ratio $f_{ce}(0)/f_{Zl}$ was typically in the range 1.5–2.5, while for locations above a minimum it was usually in the range 0.4–0.8. With this in mind, and since $f_{pe}(s)^2 \sim n_e(s)$, the above equation suggests that $dn_e(s)/ds \sim df_{ce}(s)/ds$ at the lower altitudes, and that $n_e(s)$ approaches a constant value at higher altitudes where $f_{ce}(s) \ll f_{Zl}$. The physics underlying this relationship are not yet clear. Analysis of additional cases will determine if this type of variation is typical.

5. Discussion

5.1. Notes on Z-mode trough occurrence and altitude profiles

Poleward of the plasmapause region we expect the trough minimum in f_Z to be relatively pronounced, as suggested by the diagram in Figure 4 from *Gurnett et al.*, [1983]. However, we have not yet ob-

served clear Z-mode reflections of upward propating waves in such regions, possibly due to the wide extent of the upper side of the trough in altitude and hence increased distance to reflection points. There may also be complexities in the up going wave reflection process (either within or outside a guiding duct) to be considered.

The data studied thus far suggest that Z-mode troughs deep enough to permit upward probing to distances of 5000 km or more along the field lines regularly occur within the low altitude periphery of the plasmasphere, where densities change rapidly along IMAGE orbits such as the one shown in Figure 12. Trough effects continue to be observed as IMAGE penetrates deeper into the plasmasphere and to higher altitudes, but their extent and form are not yet well known.

Along a geomagnetic field line path above IMAGE, an f_Z trough such as the one sketched in Figure 4a will have an upper edge or limit at some point between IMAGE and the equator. If the upper edge is below the equator, the f_Z curve beyond this edge will tend to fall to a minimum near the equator and then in the opposite hemisphere rise to form the upper edge of a conjugate f_Z trough (assuming symmetry of the plasma distribution around the equator). Since Z-mode waves can apparently be efficiently trapped in field aligned ducts, one can imagine various scenarios in which echoes at frequencies above the trapping region upper limit (corresponding to f_2 in Figure 4b) return from reflection points in the conjugate hemisphere. For example, a narrow range of Z-mode frequencies just above the trapping region upper limit may propagate in the Z mode to the conjugate region and return as echoes with virtual ranges that may reach 10 to 20 R_E. This may occur if the upper edge of the local trough is sufficiently close to the equator (i.e. $f_2 < f_{pe}$ at the equator). On the other hand, higher Z-mode frequencies in the f_2 range will tend to couple into the O mode at trapping region altitudes (at f_{pe} in Figure 4b). They may then propagate as O mode to a low altitude conjugate region and then couple back into the Z mode before reflection. This type of O-Z-O propagation along field line paths has been observed in RPI echo patterns [*Reinisch et al.*, 2001]. The corresponding signatures of range versus frequency can provide new insights into ducted propagation phenomena as well as additional ways of studying field line plasma distributions.

In future Z-mode work it will be of interest to increase the virtual range limits so that echoes from the conjugate region can be recorded. The large virtual ranges required, perhaps as much as 10 to 20 R_E, will force a reduction in pulse repetition rates, but there should be compensating ways of limiting sounding frequencies on the basis of acquired experience with Z-mode sounding.

5.2. Importance of wave ducts

Guiding along a discrete path excited by RPI is believed necessary in order to explain both the timing and intensity of the higher order echoes observed in a number of cases of propagation within Z-mode cavity regions. The observed widespread occurrence of ducting of O- and X-mode signals along field lines both inside and outside the plasmasphere [e.g. *Fung et al.*, 2003], as well as the range spreading consistently observed on RPI echoes not returning from the magnetic field direction [e.g. *Carpenter et al.*, 2002], suggests that Z-mode trough regions should regularly be permeated by guiding density structures. The extent and efficiency of guiding may vary widely, however. When ducting effects are present, the echoes may be discrete, as in Figures 6a and 12a, or diffuse as in Figure 6b.

5.3. Possible applications of trapped Z-mode echoes

Trapped Z-mode echoes may be used to investigate the transition

region between the auroral zone and the inner plasmasphere. This is a dynamic region, generally less well known in terms of behavior during cycles of disturbance and recovery than is the region near the magnetic equator. Some indication of the complexity of the density contours in this region can be seen in the present work. In Figure 14, for the event of Figure 6a, we find that along the field lines some 8,000 km above IMAGE, the density changed (decreased) by a factor of roughly 2, from $\approx$ 1200 el-cm^{-3} to $\approx$ 600 el-cm^{-3}. On the other hand, in the case of Figure 12, the electron density determined from changes in f_Z and f_{ce} changed (increased) by the same factor as IMAGE moved only about 2000 km inward across the magnetic field and slightly upward, as shown by the inset in Figure 1. It is clearly of importance to explore this "plasmasphere boundary layer." On a future sounding mission, it might be possible to probe the region from a near circular orbit in the 3000–5000 km range with special provision for the long virtual ranges to be expected.

6. Concluding remarks

6.1. General diagnostic applications of the Z-mode echoes

The Z mode is efficiently excited during almost all soundings in which all or part of its locally allowed frequency range falls within the band of transmitted frequencies. At medium altitudes within the plasmasphere, where the condition $f_{pe}/f_{ce} > 1$ usually obtains, discrete Z-mode echoes are observed, analogous to the regular and oblique Z-mode echoes found on topside sounder records. These may be used to probe the plasma structure earthward of IMAGE. When such measurements extend below 3000 km altitude, they may complement RPI results on field-line plasma distributions at higher altitudes obtained from X-mode echoes.

Because of the repeated appearance of Z-mode echoes in RPI plasmagrams, particularly at medium to low altitudes and over the polar regions, it appears that they can play a useful role in helping to determine local plasma parameters, by analogy to the way that stimulated plasma resonances are being used for determination of plasma parameters along high altitude portions of IMAGE orbits [*Benson et al.*, 2003]. For example, f_{uh} is rarely defined on passive recordings at low altitudes outside and near the plasmasphere and in the polar regions, but on sounding records in those regions may be readily identified. In cases such as that of Figure 5b, there are often amplitude differences of 40 dB or more between the detected levels at the high frequency limit of the Z mode (i.e. at the local f_{uh}) and at the next sounder frequency $\approx$ 10 kHz above. Within the plasmasphere, the value of f_{pe} can often be found directly from the cutoff frequency of a Z'-type trace, as in Figures 2b and 2c.

The Z mode is also of interest for purposes of investigating wave propagation in space, much along the lines originally proposed for Shuttle experiments with a subsatellite. Dispersion relations may be studied, as well as the changes in wave properties in the vicinity of f_{pe}, f_{ce}, f_Z, and f_{uh}, an example being the distinctive range decrease in diffuse Z-mode echoes that appears at f_{ce} in polar regions where $f_{pe}/f_{ce} < 1$. The scattering of Z-mode waves by irregularities may be investigated, by analogy to ways in which scattering of the free space and whistler modes has been studied [e.g. *Bell and Ngo*, 1988, 1990].

6.2. A new tool: diagnostics in a Z-mode trapping region

The existence of Z-mode trapping regions, particularly along auroral field lines, has been noted previously [e.g. *Gurnett et al.*, 1983], as well as the apparent role of the regions in trapping natural Z-mode noise. In the present work we have called attention to aspects of the trapping regions that facilitate radio sounding exper-

iments: their regular occurrence near and within the plasmasphere in the ≈ 3000–10,000 km altitude range and the presence of wave ducts that may allow transmitted Z-mode signals to propagate back and forth along the geomagnetic field.

We conclude that through analysis of the complex discrete echoes obtained in trapping regions, it should be possible to explore the profiles of those regions and hence the shapes in three dimensions of what may be called Z-mode wave cavities, volumes within and near the plasmapause where Z-mode waves can be trapped. The inferred forms of these cavities and their variations with time and disturbance levels may tell us much about the (presently poorly known) plasma distributions with altitude under the non-equilibrium (non hydrostatic) conditions that must often prevail, especially near the plasmapause.

From the limited number trapping region echoes analyzed thus far, we found the field-line density distribution above ≈ 4000 km to be such that $dn_e(s)/ds \sim df_{ce}(s)/ds$ at the lower altitudes, and that $n_e(s)$ approaches a constant value at higher altitudes. The physics underlying this relationship are not yet clear.

Although details of the shape of the f_Z trapping region must be obtained through analysis of the echo range-versus-frequency forms, including ray tracing, it appears possible to derive basic information about the f_Z altitude profile from simple inspection of the plasmagrams. This information includes: (1) the value of f_Z at the location of IMAGE and hence, after obtaining f_{ce} from RPI-stimulated resonances or from a model, the local f_{pe}; (2) the direction to the f_Z trough minimum with respect to the satellite (either below or above it)(from the echo forms on the plasmagrams); (3) the value of f_Z (and hence, after using a model f_{ce}), f_{pe}) at the upper limit of the trough (from the upper frequency limits of the B or D echoes).

Most of the Z-mode activity reported above has been incidental to sounding experiments designed for the free space modes. It is now clear that Z-mode echoes from RPI have substantial diagnostic potential and should be included with the free space modes as a regular RPI diagnostic tool.

Appendix A: A Z-mode inversion method

The virtual range of the reflection point of a ducted Z-mode signal can be related to the actual range s through the relation:

$$R(f) = c \int_o^s ds/V_g(f, f_{ce}(s), f_{pe}(s)) \qquad (1)$$

where ds is a differential element of path length, $V_g(f, f_{ce}, f_{pe}, s)$ is the group velocity of the Z-mode signal along the duct, f is the signal frequency, $f_{ce}(s)$ is the electron gyrofrequency, $f_{pe}(s)$ is the electron plasmafreqency, and c is the free-space speed of light [*Jackson*, 1969]. The refractive index of a Z-mode signal propagating in a duct parallel to the Earth's magnetic field B_o has the value:

$$n = [1 - f_{pe}^2/(f^2 + f f_{ce})]^{1/2} \qquad (2)$$

where for simplicity the explicit dependence of f_{ce} and f_{pe} upon s is suppressed and the small range of angles around **B** to which a ducted wave should be confined [e.g., *Calvert*, 1995] is taken to be zero.

The group velocity can be determined from the relation:

$$V_g = \partial\omega/\partial k \qquad (3)$$

where ω is the angular wave frequency, $k = n\omega/c$. By combining (2) and (3), we can express V_g in the following convenient form:

$$V_g = c[f^2 + f f_{ce} - f_{pe}^2]^{1/2}/h(f, f_{ce}, f_{pe}) \quad (4)$$

where:

$$h(f, f_{ce}, f_{pe}) = [f^2 + f f_{ce}]^{1/2}[1 - \frac{(f_{pe}^2 f_{ce})}{2f(f_{ce} + f)^2}]. \quad (5)$$

In the cases of Z-mode propagation we are considering, the frequency range of the Z-mode signals is very small compared to the magnitude of the wave frequency. For example in Figure 8 it can be seen that the frequencies of the propagating Z-mode signals are $\sim$ 400 kHz, while the frequency range of propagation is $\sim$ 40 kHz. Over this small frequency range the function $h(f, f_{ce}, f_{pe})$ varies very little.

Furthermore we can reasonably approximate the frequency-dependent terms within the square root of V_g through the use of a two term Taylor series expansion about the local Z-mode cutoff frequency f_{Zl}, where:

$$f_{Zl} = [f_{pel}^2 + f_{cel}^2/4]^{1/2} - f_{cel}/2, \quad (6)$$

and where f_{cel} is the local electron gyrofrequency and f_{pel} is the local electron plasma frequency at the spacecraft. With these approximations we obtain:

$$V_g = c[(2f + f_{ce})(f - f_{Zl}) - f_{pe}^2]^{1/2}/h(f_{Zl}, f_{ce}, f_{pe}). \quad (7)$$

It is useful to define a new function $g(s)$, where:

$$g(s) = [f_{pe}^2(s) - f_{Zl} f_{ce}(s) - f_{Zl}^2]/[f_{Zl} f_{ce}(s) + 2f_{Zl}^2]. \quad (8)$$

If we now eliminate f_{pe}^2 using $g(s)$ we arrive at a new form for (1):

$$R(f) = \int_o^s t(s)ds/[\delta(f) - g(s)]^{1/2}, \quad (9)$$

where $\delta(f) = (f - f_{Zl})/f_{Zl}$ and:

$$t(s) = 0.5\frac{[f_{ce} + 2f_{Zl}]^{1/2}}{[f_{ce} + f_{Zl}]^{1/2}} + 0.5\ g(s)\frac{f_{ce}[f_{ce} + 2f_{Zl}]^{1/2}}{[f_{ce} + f_{Zl}]^{3/2}}. \quad (10)$$

We note that $g(0) = 0$, and in general we expect $g(s)$ to be small because at every point along the propagation path the Z-mode signal frequency is always close to the local Z-mode cutoff frequency at the spacecraft. For example from Figure 8 it can be shown that the maximum value of $g(s) = (f - f_{Zl})/f_{Zl}$ is less than 8 %. In general it can be shown that the ratio of the second term in (10) to the first is always less than $g(s)$. Thus when $g(s)$ is small, the second term in (10) can be neglected.

To find the solution to (9) when the second term in (10) is negligible, we follow a technique described in detail in *Budden* [1985, pages 337-342]. we first note that in general if we pick a particular value for $g(s)$, i.e., $g(s) = g'$, there will be a particular range R' associated with this value and a particular signal frequency f' since at the reflection point $g' = (f' - f_{Zl})/f_{Zl}$. With this in mind, we multiply both sides of (9) by the factor $[f' - f]^{-1/2}$ and integrate from $f = f_{Zl}$ to $f = f'$. The following expression obtains:

$$\int_{f_{Zl}}^{f'} \frac{R(f-f_{Zl})df}{[f'-f]^{1/2}} = \int_{f_{Zl}}^{f'} \int_{o}^{s} \frac{t_o(s)dsdf}{[\delta(f)-g(s)]^{1/2}[f'-f]^{1/2}}, \tag{11}$$

where $t_o(s) \sim 0.5 \frac{[f_{ce}+2f_{Zl}]^{1/2}}{[f_{ce}+f_{Zl}]^{1/2}}$.

On the right hand side of (11) we now interchange the integrations and perform the frequency integration first. On the left hand side we make the substitution $f = f_{Zl} + (f' - f_{Zl})\sin(\alpha)^2$ and integrate over α. This action results in the following expression for monotonically varying z mode traces, such as that exhibited by the upward propagating z mode signals in Figure (8), which have zero range at $f = f_{Zl}$:

$$\frac{2\delta(f')^{1/2}}{\pi} \int_{0}^{\pi/2} R(f_{Zl}\,\delta(f')\,\sin\alpha^2)\sin\alpha d\alpha = \int_{o}^{s} t_o(s)ds \tag{12}.$$

Since the value of f' is arbitrary and $t_o(s)$ is a known function of s, (12) represents the implicit solution for $g(s)$. For example, if we pick a value for f', this defines g' through the relation $g' = (f' - f_{Zl})/f_{Zl}$. We then evaluate the lhs of (12) to obtain its numerical value for the given f'. We then perform the integration on the rhs of (12) until the right and left sides are equal. The value of s at which this equality obtains is then the range at which $g(s) = g'$. At this point the value of f_{pe}^2 at this range can be found from (8), since $f_{ce}(s)$ is a known function of s.

Finding the solution for $g(s)$ is more difficult when the Z-mode signal from the spacecraft propagates across the Z-mode cavity, across the altitude at which f_Z has a minimum, reflects from the opposite side of the cavity and returns to the spacecraft. Typical examples of Z-mode traces resulting from this type of propagation are shown in Figure 6, where the virtual range of the reflected signal for $f{=}f_{Zl}$ is $\sim 1.5\ R_E$. For these cases, from (9), the virtual range at $f{=}f_{Zl}$ becomes:

$$R_o = R(f{=}f_{Zl}) = \int_{o}^{s_o} t_o(s)ds/[-g(s)]^{1/2}, \tag{13}$$

where s_o is the true range of the first reflection point across the Z-mode cavity, and where $g(s) \leq 0$ for $0 \leq s \leq s_o$. Although (13) gives some information concerning $g(s)$ within the Z-mode cavity, it is not enough to determine $g(s)$ or even s_o.

To attempt the solution of (9) for cases such as those shown in Figure 6, we follow the same steps outlined above with respect to (12) to find the relation:

$$\frac{2\delta(f)^{1/2}}{\pi} \int_{0}^{\pi/2} R(f_{Zl}\,\delta(f)\,\sin\alpha^2)\sin\alpha d\alpha$$
$$= \int_{o}^{s} t_o(s)ds - \frac{2}{\pi}\int_{o}^{s_o} t_o(s)\arctan(-g(s)/\delta(f))^{1/2}ds. \tag{14}$$

Equation (14) represents an integral equation relating the function $g(s)$ within the Z-mode cavity to the virtual range and the signal frequency. Comparing (12) with (14), it can be seen that (14) contains an extra term on the right hand side. As explained in *Budden* [1985], the extra term arises because $g(s)$ is not a monotonically increasing function of s within the propagation region. We can neglect the extra term if $s_m \gg s_o$, where s_m is the maximum range for the highest frequency. To estimate the magnitude of s_o, We solve (9) using a trial function for $g(s)$ within the cavity. We require that $g(s) = 0$ for $s = 0$ and $s = s_o$ and $g(s) \leq 0$ between these points, that $g(s)$ be continuous at these points, and that (13) is finite. A simple function that satisfies these requirements is:

$$g_c(s) = \lambda s(s - s_o) \tag{15}$$

where $g_c(s)$ is the value of $g(s)$ within the cavity and λ is a constant. Using (15) in (9) we obtain to first order:

$$R(f) \sim [\lambda]^{-1/2} t_o(0)(\pi - \frac{2}{s_o}[\frac{\delta(f)}{\lambda}]^{1/2}). \tag{16}$$

We now note that the constant λ can be found from (16) through the relation:

$$R(f = f_{Zl}) = \pi[\lambda]^{-1/2} t_o(0), \tag{17}$$

where for example in the case of Figure 6, $R(f = f_{Zl}) \sim 1.5 R_E$. Furthermore if we fit (16) to the initial portion of the lower Z-mode trace of Figure 6, we also find that $s_o \sim 1300$ km. Thus for our trial function (15), if $s_m \gg 1300$ km, then the last term in (14) is negligible.

In general, the true range of upward propagating ducted Z-mode signals within a Z-mode cavity is limited either by the finite extent of the duct along B_o or the finite extent of the cavity. In the case in which the cavity is the limiting factor, it can be shown from (1) that $\lim_{f \to f_{Zm}} R(f) = \infty$, where f_{Zm} is the maximum value of f_Z above the spacecraft. Thus the virtual range becomes arbitrarily large as f approaches f_{Zm}, and the slope of the curve becomes vertical. This type of behavior is exhibited by the two upward propagating Z-mode signal traces ('D' traces) in Figure 8. On the other hand, the two upward propagating Z-mode signal traces in Figure 6 ('B' traces) do not show this asymptotic behavior and terminate abruptly with slopes of $\sim 45°$. In these cases the limiting factor may be the breakdown of ducting. The conditions under which ducting of Z-mode signals is possible have been discussed by *Calvert* [1995].

Acknowledgments. The work at University of Massachusetts Lowell was supported by NASA under a subcontract from Southwest Research Institute. The work at Stanford University was supported by subcontract no. 03-08482 from the University of Massachusetts Lowell.

References

Bell, T. F., and H. D. Ngo, Electrostatic waves stimulated by coherent VLF signals propagating in and near the inner radiation belt, *J. Geophys. Res., 93*, 2599, 1988.

Bell, T. F., and H. D. Ngo, Electrostatic lower hybrid waves excited by electromagnetic whistler mode waves scattering from planar magnetic-field-aligned irregularities, *J. Geophys. Res., 95*, 149, 1990.

Benson, R. F., Auroral kilometric radiation: wave modes, harmonics, and source region electron density structures, *J. Geophys. Res., 90*,, 2753, 1985.

Benson, R. F., Stimulated plasma waves in the ionosphere, *Radio Science, 12*, 861, 1977.

Benson, R. F., Elusive upper hybrid waves in the auroral topside ionosphere, in *Auroral Plasma Dynamics, Geophysical Monograph 80*, American Geophysical Union, 1993.

Benson, R. F., V. A. Osherovich, J. Fainberg, and B. W. Reinisch, Classification of IMAGE/RPI-stimulated plasma resonances for the accurate determination of magnetospheric electron-density and magnetic field values, *J. Geophys. Res., 108*, 2003.

Burch, J. L., IMAGE mission overview, *Space Science Reviews, 91*, 1, 2000.

Budden, K. G., *The propagation of radio waves*, Cambridge University Press, 1985.

Calvert, W., Oblique Z-mode echoes in the topside ionosphere, *J. Geophys. Res., 86*, 1609, 1981.

Calvert, W., Wave ducting in different wave modes, *J. Geophys. Res., 100*, 17491, 1995.

Calvert, W., and J. R. McAfee, Topside sounder resonances, *Proc. IEEE, 57*, 1019, 1969.

Carpenter, D. L., and R. R. Anderson, An ISEE/whistler model of equatorial electron density in the magnetosphere, *J. Geophys. Res., 97*, 1097, 1992.

Carpenter, D. L., M. A. Spasojević, T. F. Bell, U. S. Inan, B. W. Reinisch, I. A. Galkin, R. F. Benson, J. L. Green, S. F. Fung, and S. A. Boardsen, Small-scale field-aligned plasmaspheric density structures inferred from the Radio Plasma Imager on IMAGE, *J. Geophys. Res., 107*,(A9), 1258, doi:10.1029/2001JA009199, 2002.

Dyson, P. L., Operational modes for a wave injection facility aboard spacelab and a sub-satellite, NASA Technical Memorandum 79657, GSFC, 1978.

Franklin, C. A., and M. A. MacLean, The design of swept-frequency topside sounders, *Proc. IEEE, 57*, 897, 1969.

Fredricks, R. W. et al., Report of the AMPS wave injection facility definition team, TRW no. 3247-6002-RU-01, 1978.

Fung, S. F., R. F. Benson, D. L. Carpenter, J. L. Green, V. Jayanti, I. A. Galkin, and B. W. Reinisch, Guided echoes in the magnetosphere: observations by Radio Plasma Imager on IMAGE, *Geophys. Res. Lett., 30* in press, 2003.

Galkin, I, G. Khmyrov, A. Kozlov, B. Reinisch, X. Huang, and G. Sales, New tools for analysis of space-borne sounding data, in *Proc. 2001 USNC/URSI National Radio Science Meeting, July 8-13, 2001,* p.304, 2001.

Gendrin, R., Waves and wave-particle interactions in the magnetosphere, *Space Sci. Rev., 18*, 145, 1975.

Goertz, C. K., and R. J. Strangeway, Plasma Waves, in *Introduction to Space Physics*, M. G. Kivelson and C. T. Russell, eds., Cambridge University Press, 1995.

Gurnett, D. A., S. D. Shawhan, and R. R. Shaw, Auroral hiss, Z-mode radiation, and auroral kilometric radiation in the polar magnetosphere: DE 1 observations, *J. Geophys. Res., 88*,, 329, 1983.

Hagg, E. L., E. J. Hewens, and G. L. Nelms, The interpretation of topside sounder ionograms, *Proc. IEEE, 57*, 949, 1969.

Huang, X., B. W. Reinisch, P. Song, P. Nsumei, J. L. Green, D. L. Gallagher, Empirical models of the plasma density in the inner magnetosphere, submitted to *Adv. Space Res.*, 2003.

Inan, U. S., T. F. Bell, R. A. Helliwell, and J. P. Katsufrakis, A VLF transmitter on the Space Shuttle, *Adv. Space Res., 1*, 235, 1981.

Jackson, J. E., The reduction of topside ionograms to electron-density profiles, *Proc. IEEE, 57*,, 960, 1969.

James, H. G., Wave propagation experiments at medium frequencies between two ionospheric satellites 3. Z-mode pulses, *J. Geophys. Res., 84*, 499, 1979.

Jones, D., Source of terrestrial non-thermal radiation, *Nature, 260*, 686, 1976.

Jones, D., Mode-coupling of Z-mode waves as a source of terrestrial kilometric and Jovian decametric radiations, *Astron. Astrophys. 55*, 245, 1977.

Kennel, C. F., and H. E. Petschek, Limit on stably trapped particle fluxes, *J. Geophys. Res., 71*,1, 1966.

LaBelle, J. W., and R. A. Treumann, Auroral radio emissions, *Space Sci. Rev., 101*, 295, 2002.

Muldrew, D. G., Nonvertical propagation and delayed-echo generation observed by the topside sounders, *Proc. IEEE, 57*, 1097, 1969.

Reinisch, B.W., Modern Ionosondes, in *Modern Ionospheric Science*, Eds. H. Kohl, R. Ruster, and K. Schlegel, European Geophysical Society, 37191 Katlenburg-Lindau, Germany, 440- 458, 1996.

Reinisch, B. W., D. M. Haines, K. Bibl, G. Cheney, I. A. Galkin, X. Huang, S. H. Myers, G. S. Sales, R. F. Benson, S. F. Fung, J. L. Green, W. W. L. Taylor, J.-L. Bougeret, R. Manning, N. Meyer-Vernet, M. Moncuquet, D. L. Carpenter, D. L. Gallagher, and P. Reiff, The Radio Plasma Imager investigation on the IMAGE spacecraft, *Space Science Reviews, IMAGE special issue, 91*, 319-359, February 2000.

Reinisch, B. W., X. Huang, D. M. Haines, I. A. Galkin, J. L. Green, R. F. Benson, S. F. Fung, W. W. L. Taylor, P. H. Reiff, D. L. Gallagher, J.-L. Bougeret, R. Manning, D. L. Carpenter, and S. A. Boardsen, First results from the radio plasma imager on IMAGE, *Geophys. Res. Lett., 28*, 1167, 2001a.

Reinisch, B. W., X. Huang, P. Song, G. S. Sales, S. F. Fung, J. L. Green , D. L. Gallagher, and V. M. Vasyliunas, Plasma density distribution along the magnetospheric field: RPI observations from IMAGE, *Geophys. Res. Lett., 28*, 4521, 2001b.

Santolík, O., F. Lefeuvre, M. Parrot, and J. L. Rauch, Propagation of Z-mode and whistler-mode emissions observed by Interball 2 in the nightside auroral region, *J. Geophys. Res., 106*, 21137, 2001.

Sonwalkar, V. S., Magnetospheric LF- VLF-, and ELF-waves, in *Handbook of Atmospheric Electrodynamics*, H. Volland, ed., CRC Press, 1995.

Sonwalkar, V. S., D. L. Carpenter, T. F. Bell, M. A. Spasojević, U. S. Inan, R. F. Benson, W. W. L. Taylor, B. W. Reinisch, Whistler mode echoes from radio sounding on the IMAGE satellite, submitted to *Radio Sci.*, 2003.

and then LaTeX to agu.bst which for BiBTeX.

(Received _____.)

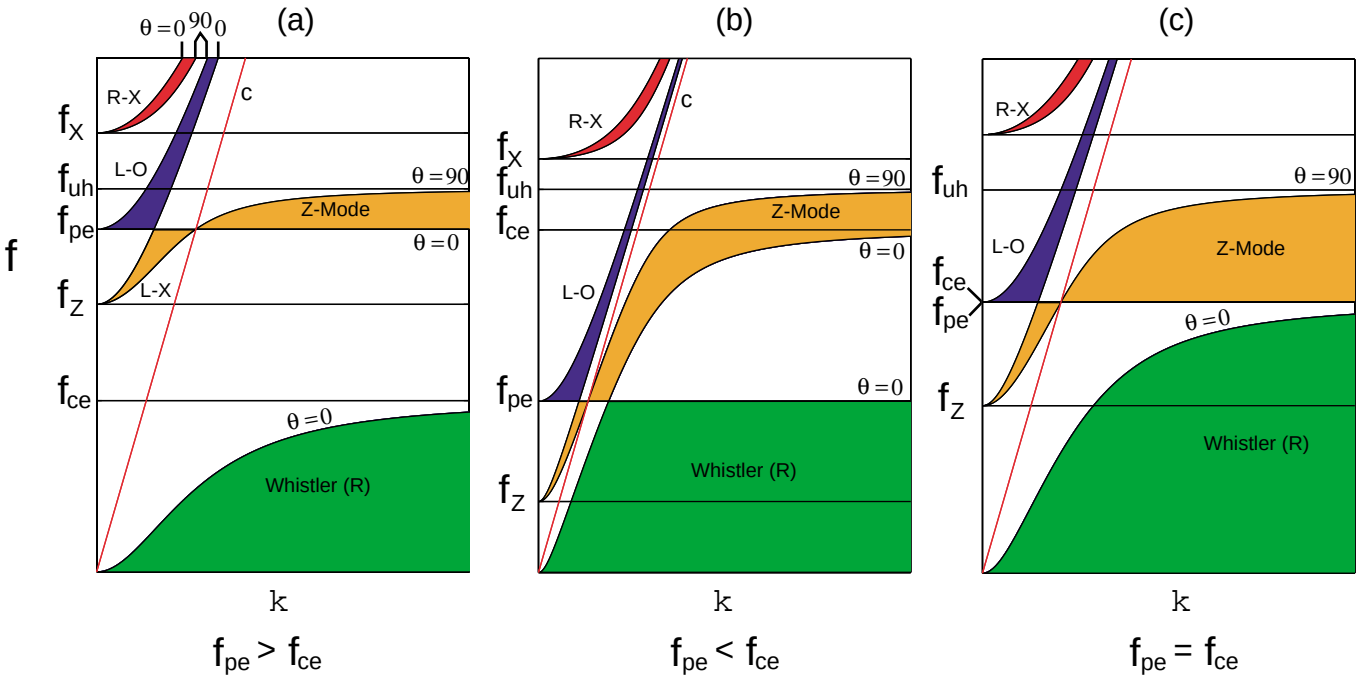

Figure 1. Dispersion diagrams, in coordinates of wave frequency f versus wave number k, showing regions of oblique propagation in various modes. (a) Diagram for the case of electron plasma frequency f_{pe} greater than the electron gyrofrequency f_{ce}. (b) Diagram for the case of f_{pe}/f_{ce} <1. (c) Diagram for the case of f_{pe}/f_{ce} =1. Adapted from *Goertz and Strangeway*, [1995].

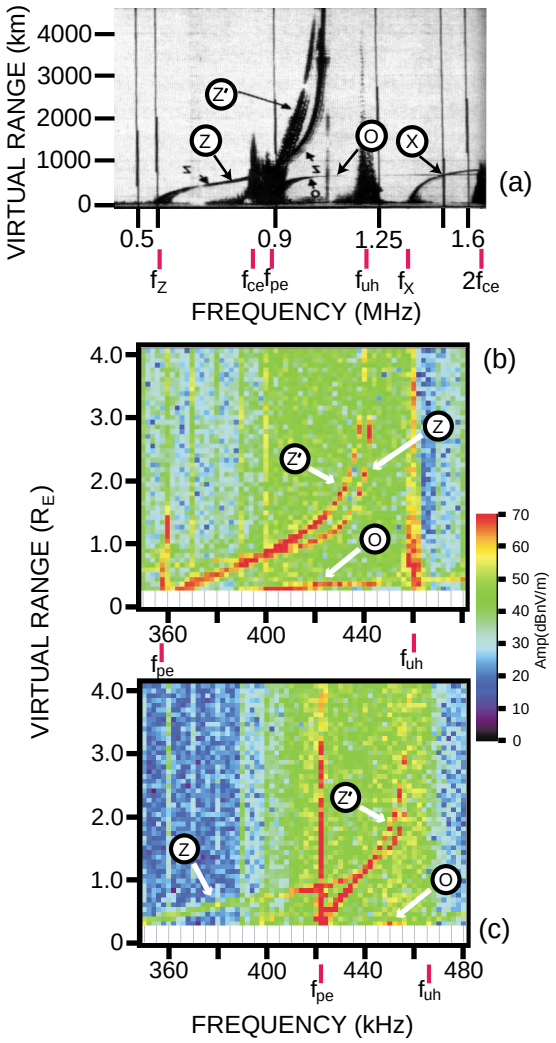

Figure 2. Comparison of Z-mode echo records from Alouette 2 (above) and from RPI on IMAGE. The Alouette data were recorded on April 6, 1966 at 1555 UT, the IMAGE data on July 6, 2001 at 1841 and 1846 UT. (a) Alouette 2 ionogram expanded in frequency and with range plotted upward for comparison with the RPI plasmagrams below. Two Z-mode echoes are shown (marked Z and Z′), as well as O- and X-mode echoes, detected at ≈ 870 km altitude. (b)and (c) RPI plasmagrams showing Z-mode echoes observed in the plasmasphere where $f_{pe}/f_{ce} > 1$. The echoes are generally similar in form to those from Alouette, but were detected at 3100 and 4100 km altitude.

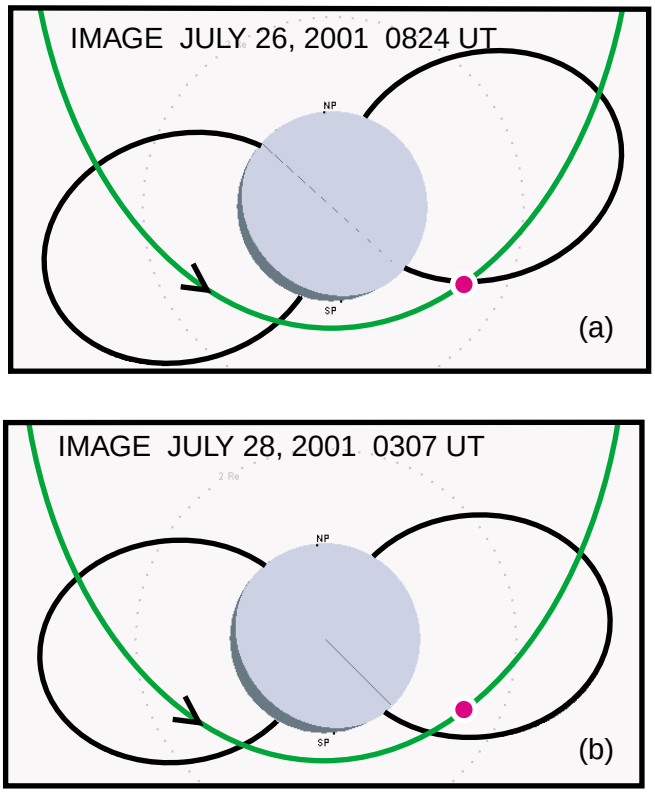

Figure 3. Plots of IMAGE orbit near perigee showing where trapped Z-mode echoes have been observed. The approximate location of the plasmapause in the late afternoon local time sector is indicated. (a) A case of Z-mode sounding from below a minimum in the Z-mode cutoff frequency profile with altitude. (b) A case of Z-mode sounding from above a minimum in the Z-mode cutoff frequency profile with altitude.

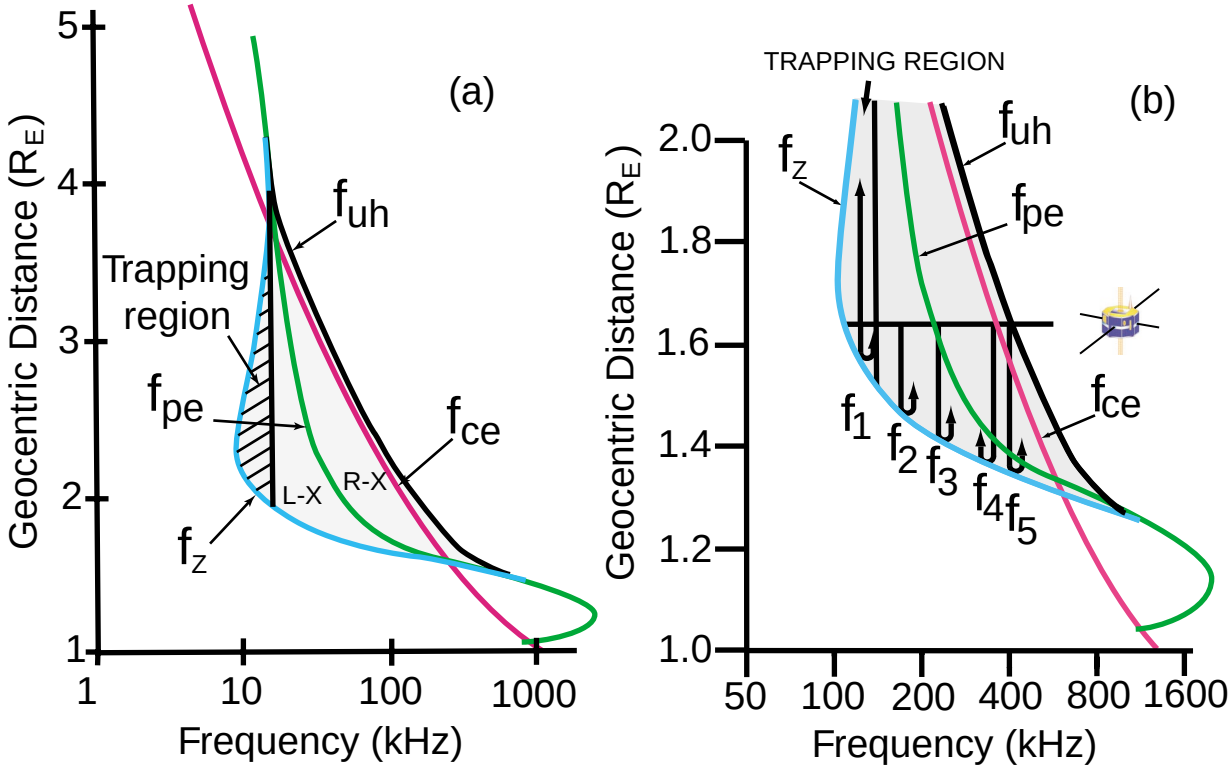

Figure 4. (a) Model plot of the variation with geocentric distance along polar region field lines of key plasma parameters, showing by shading the Z-mode trapping region (adapted from *Gurnett et al.*, [1983]).(b) Modified version of Figure 4a illustrating, for a particular case of sounding by RPI, a number of idealized ray paths for Z-mode echoes

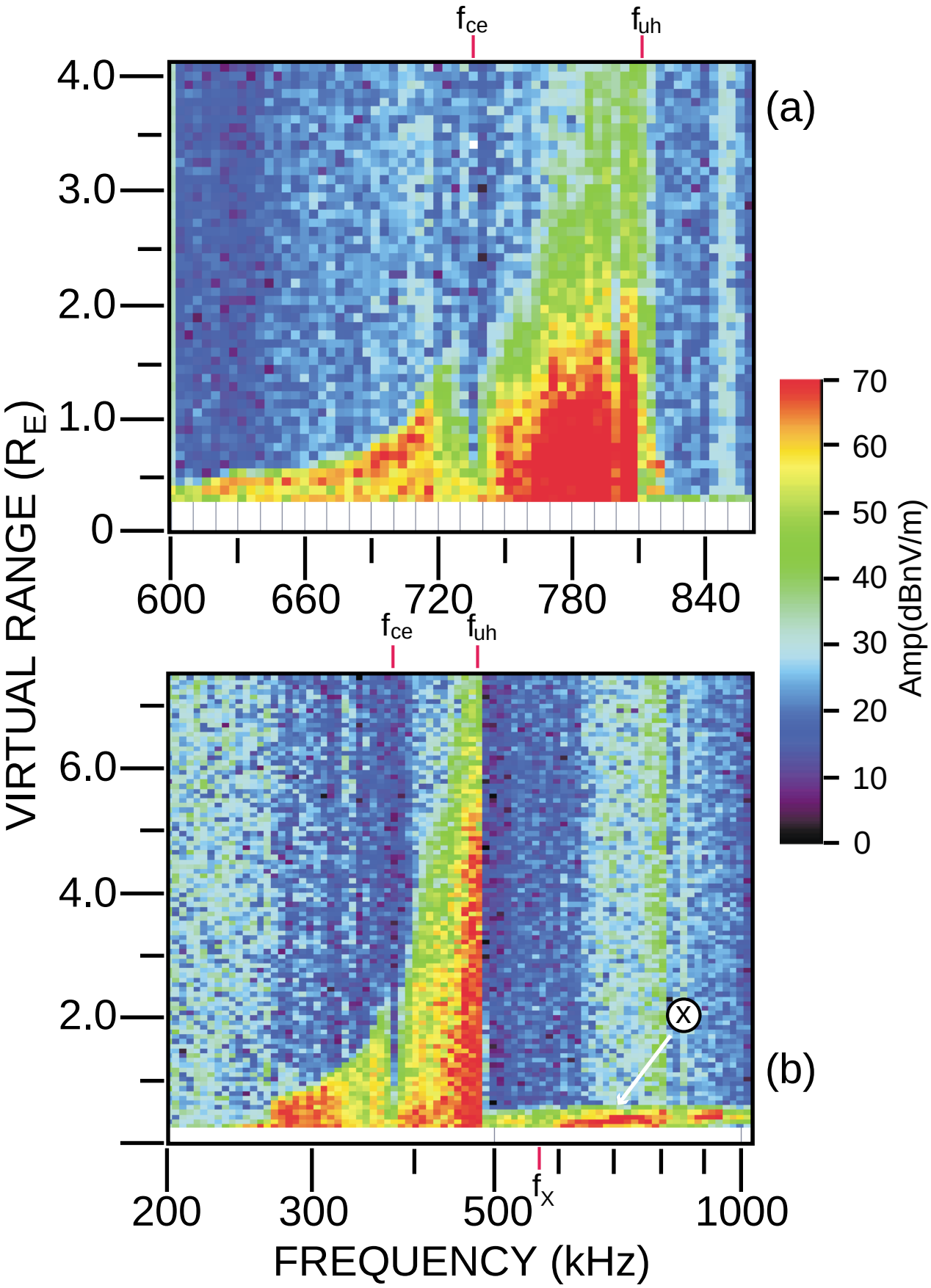

Figure 5. RPI plasmagrams from July 4, 2001, 0931 UT, and February 22, 2002, 1054 UT, showing Z-mode echoes detected near perigee in southern polar regions under conditions of $f_{pe}/f_{ce} < 1$. (a) Echoes from sounding at $\approx$ 1500 km. (b) Echoes from sounding at $\approx$ 3400 km.

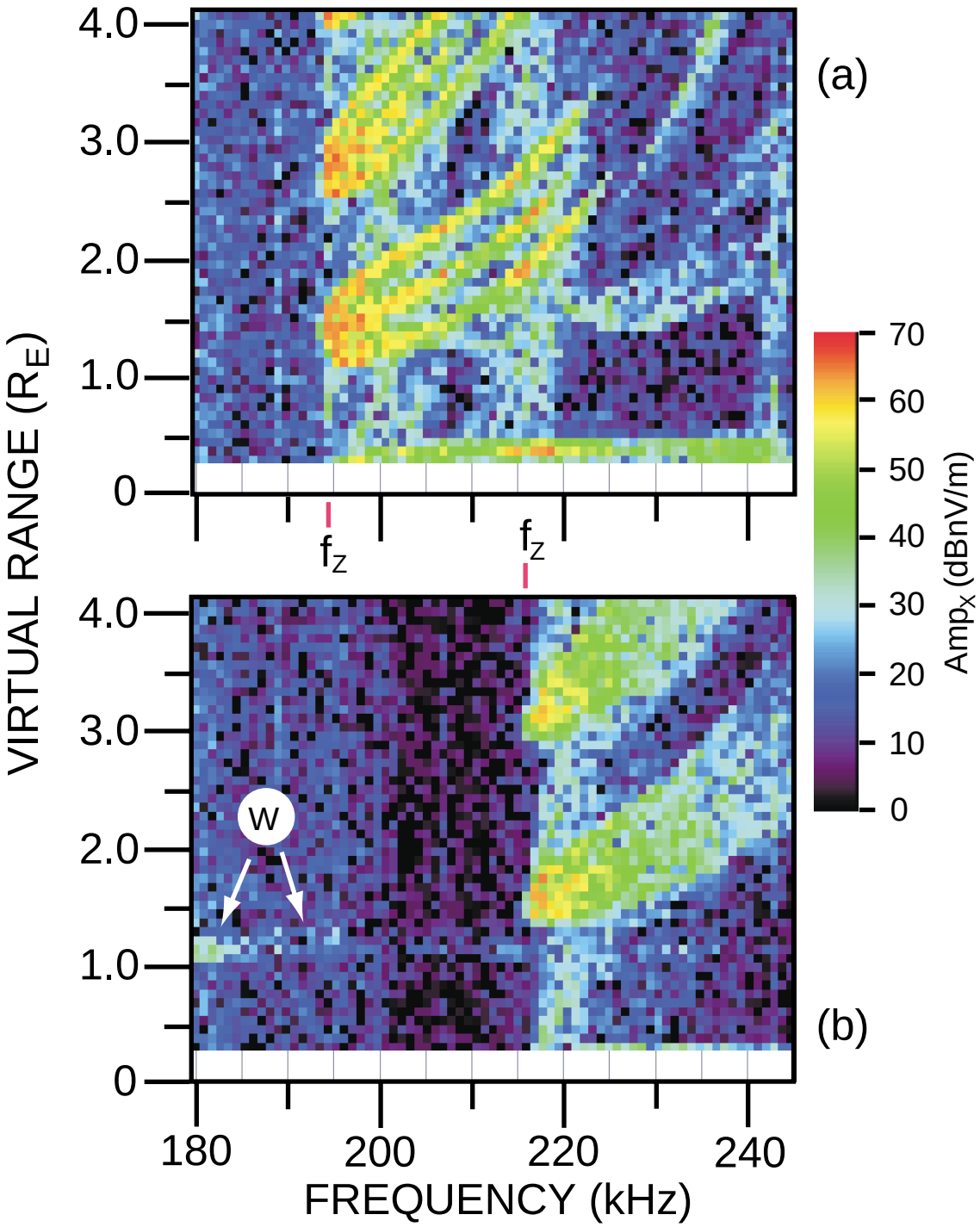

Figure 6. RPI plasmagrams from July 26, 2001, 0824 UT and July 12, 2001, 0245 UT, showing multi-component Z-mode echoes detected in the region of density gradients between the southern auroral zone and the plasmasphere. The approximate location of IMAGE is indicated in Figure 3a. Whistler-mode echoes due to reflections from the bottom side of the ionosphere are marked "W" and appear at the lower left in the bottom record.

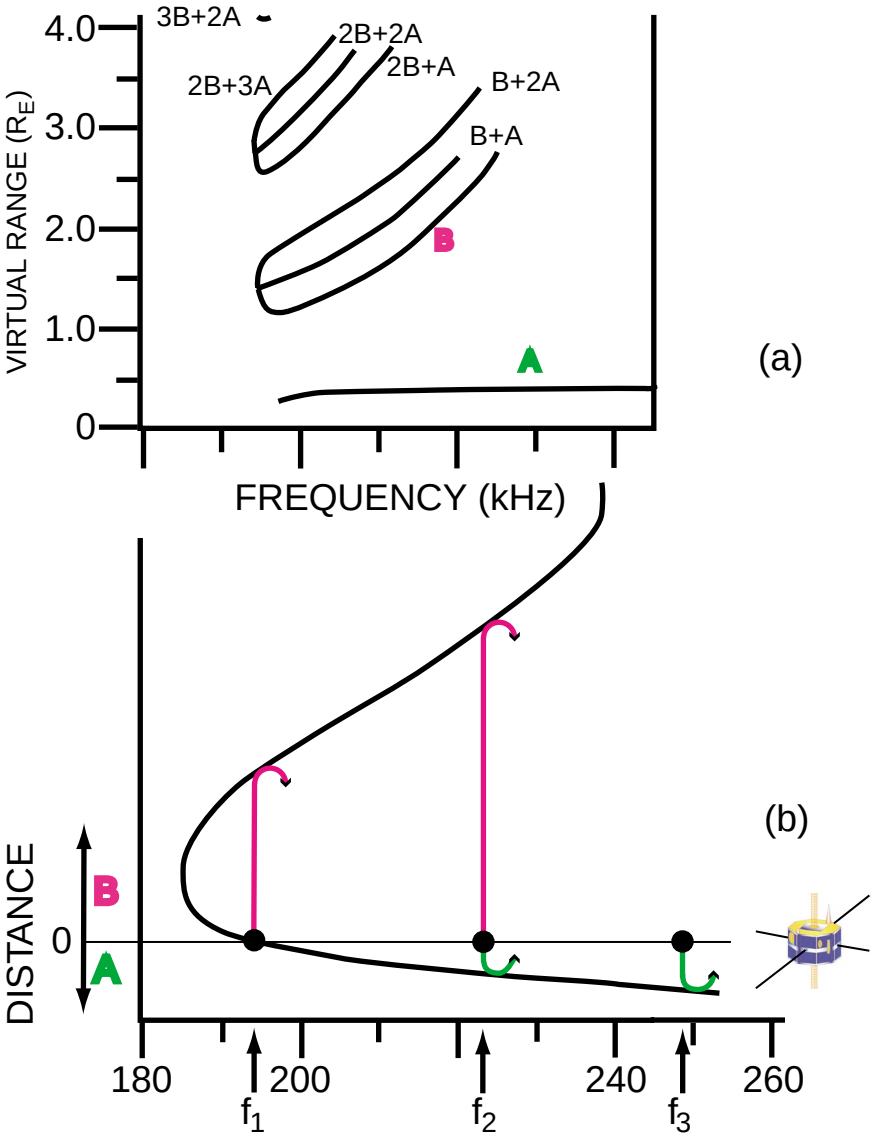

Figure 7. Interpretive model of the echoes of Figure 6a. (a) Tracing of the principal echo elements in virtual range versus frequency. (b) Diagram of proposed echo paths when the sounder is located below a minimum in Z-mode cutoff frequency with altitude.

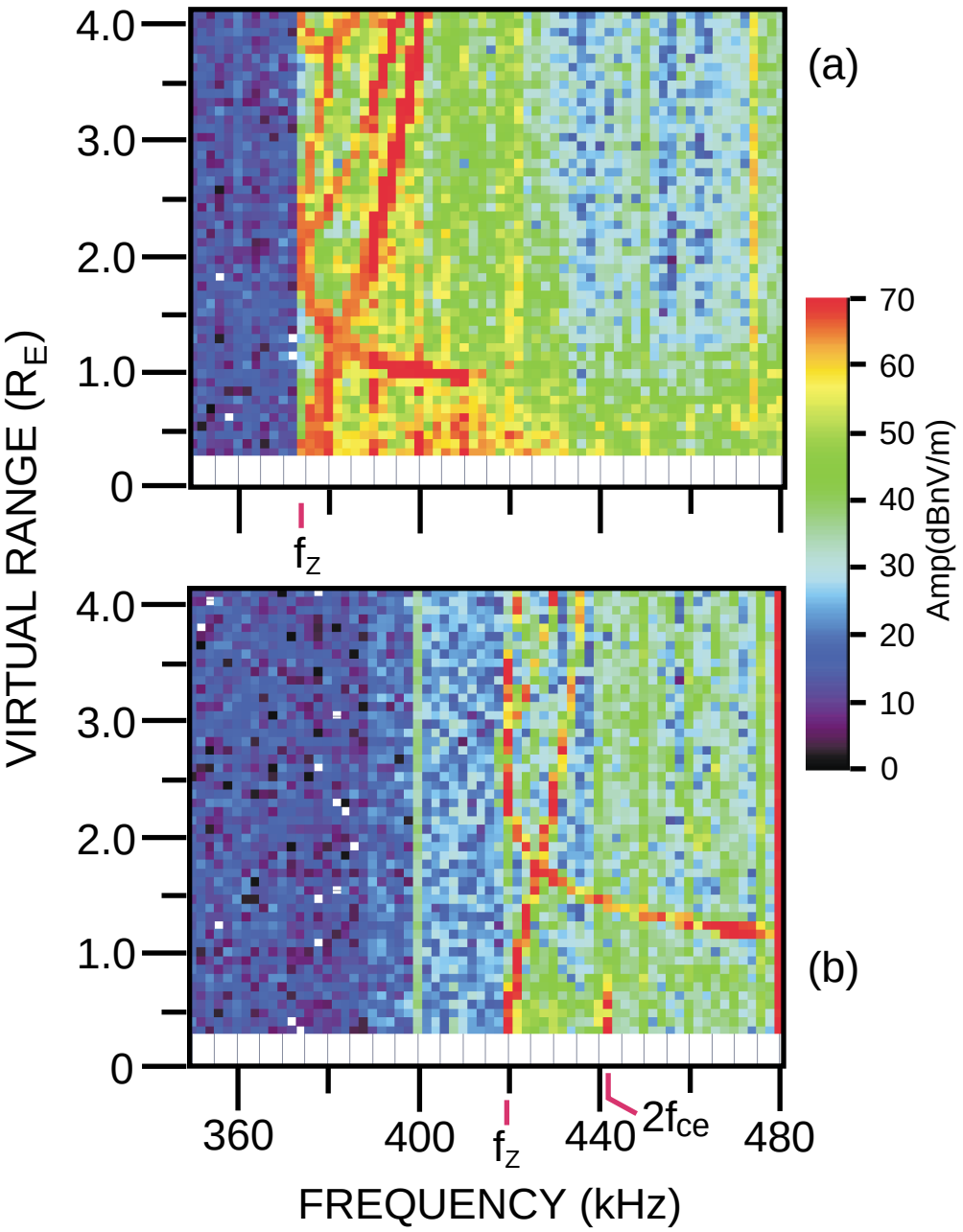

Figure 8. RPI plasmagrams from July 28, 2001 at ≈ 0308 UT, showing multi-component Z-mode echoes detected within the plasmasphere on successive soundings 2 1/2 min apart. The approximate location of IMAGE is indicated in Figure 3b.

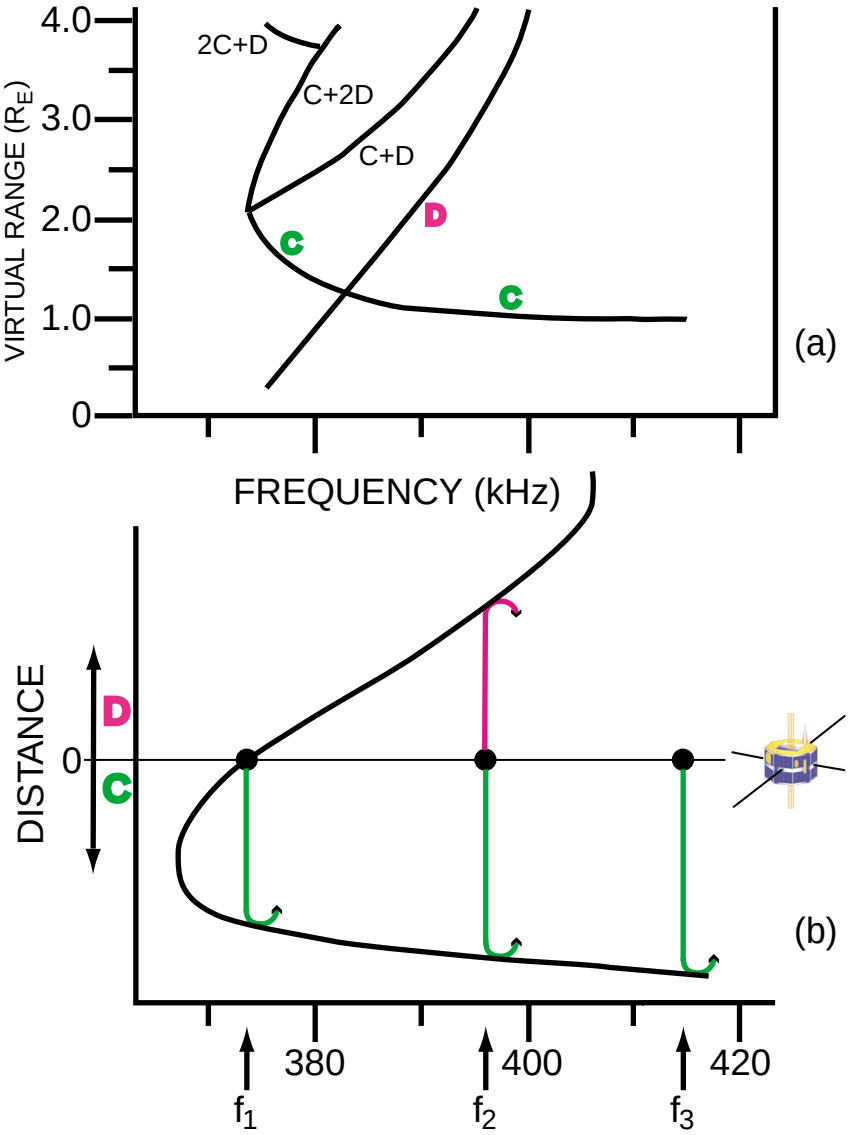

Figure 9. Interpretive model of the echoes of Figure 8a, similar to that in Figure 7, but for the case of a sounder location above the minimum in Z-mode cutoff frequency with altitude.

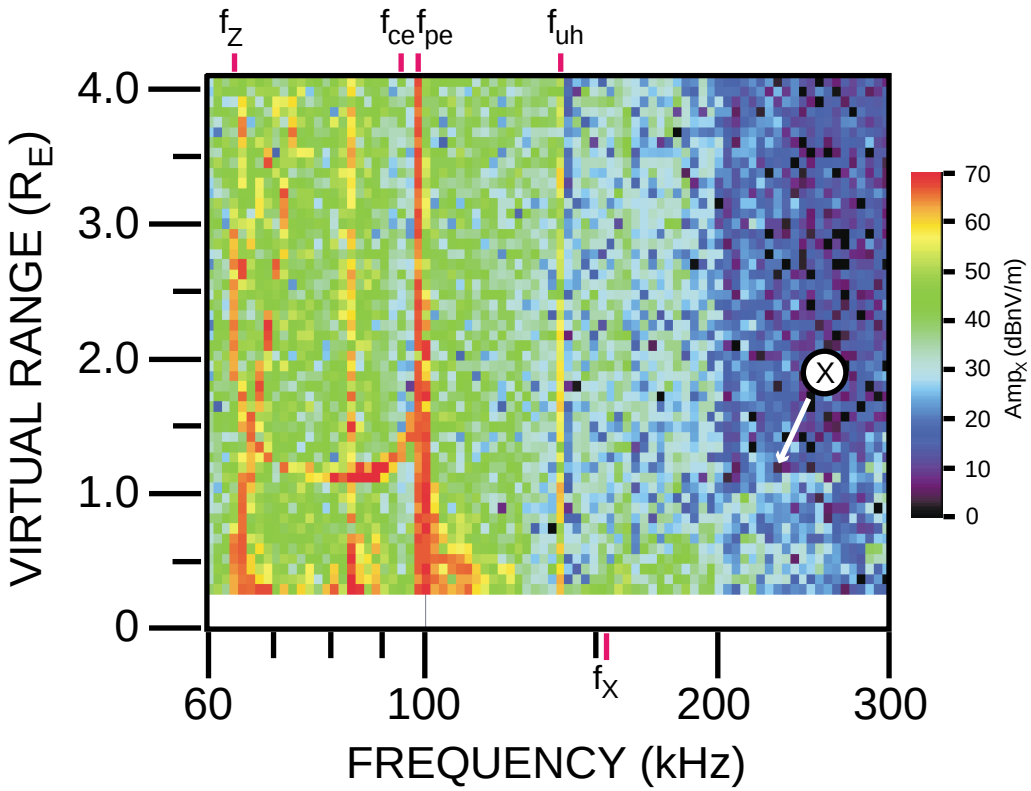

Figure 10. Example of a multi-hop Z-mode echoing event detected on May 14, 2002, 0130 UT, at 9300 km altitude as IMAGE was moving through a region of plasmapause-associated density gradients.

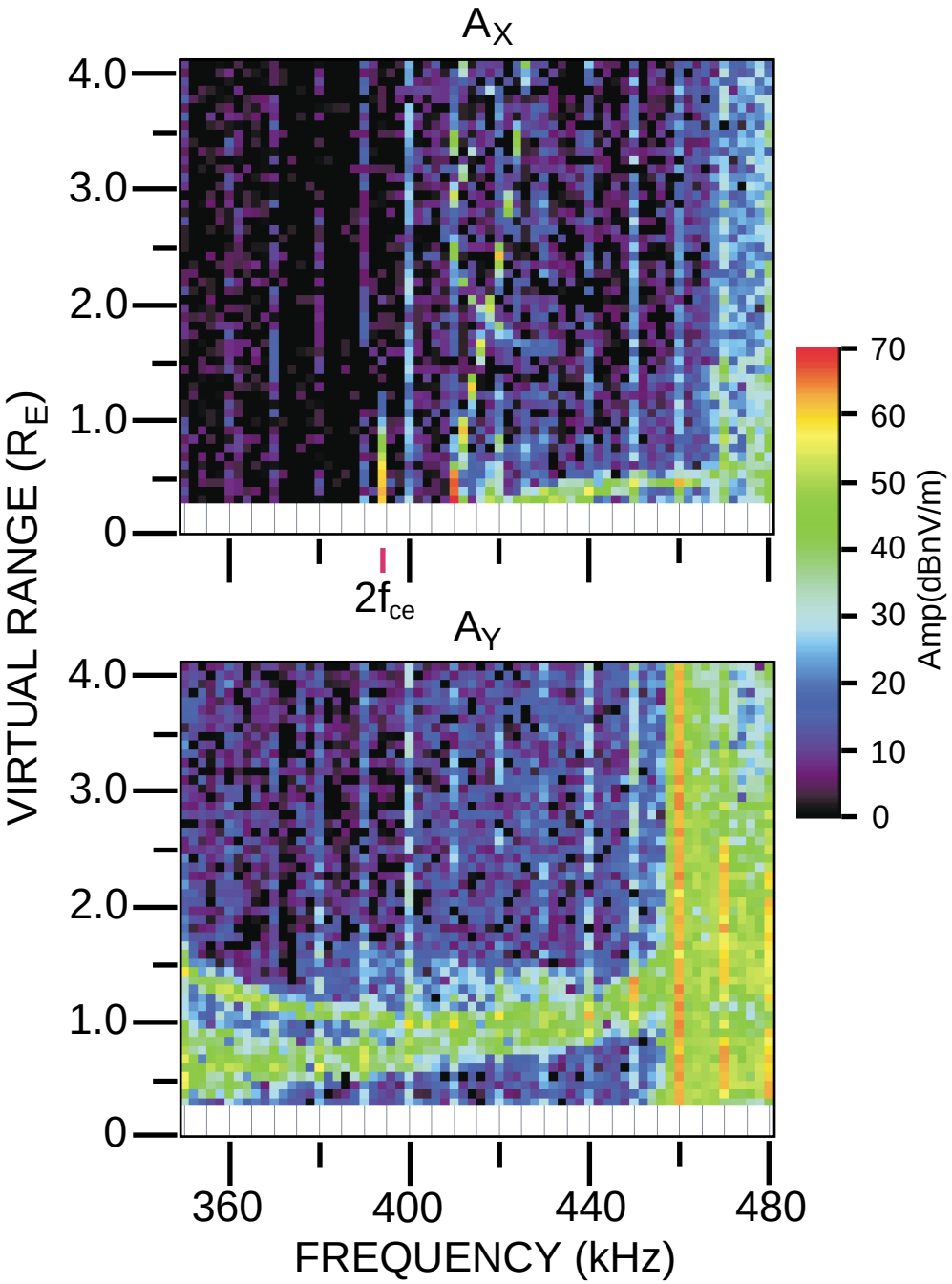

Figure 11. Examples of trapped Z-mode echoes accompanied by direct echoes, i.e. ones that followed ray paths such that a minimum in the Z-mode cutoff frequency with altitude was not encountered. The two cases are from July 23, 2001, 2252 UT (above) and 0922 UT. The vertical striations at multiples of 10 kHz are due to interference.

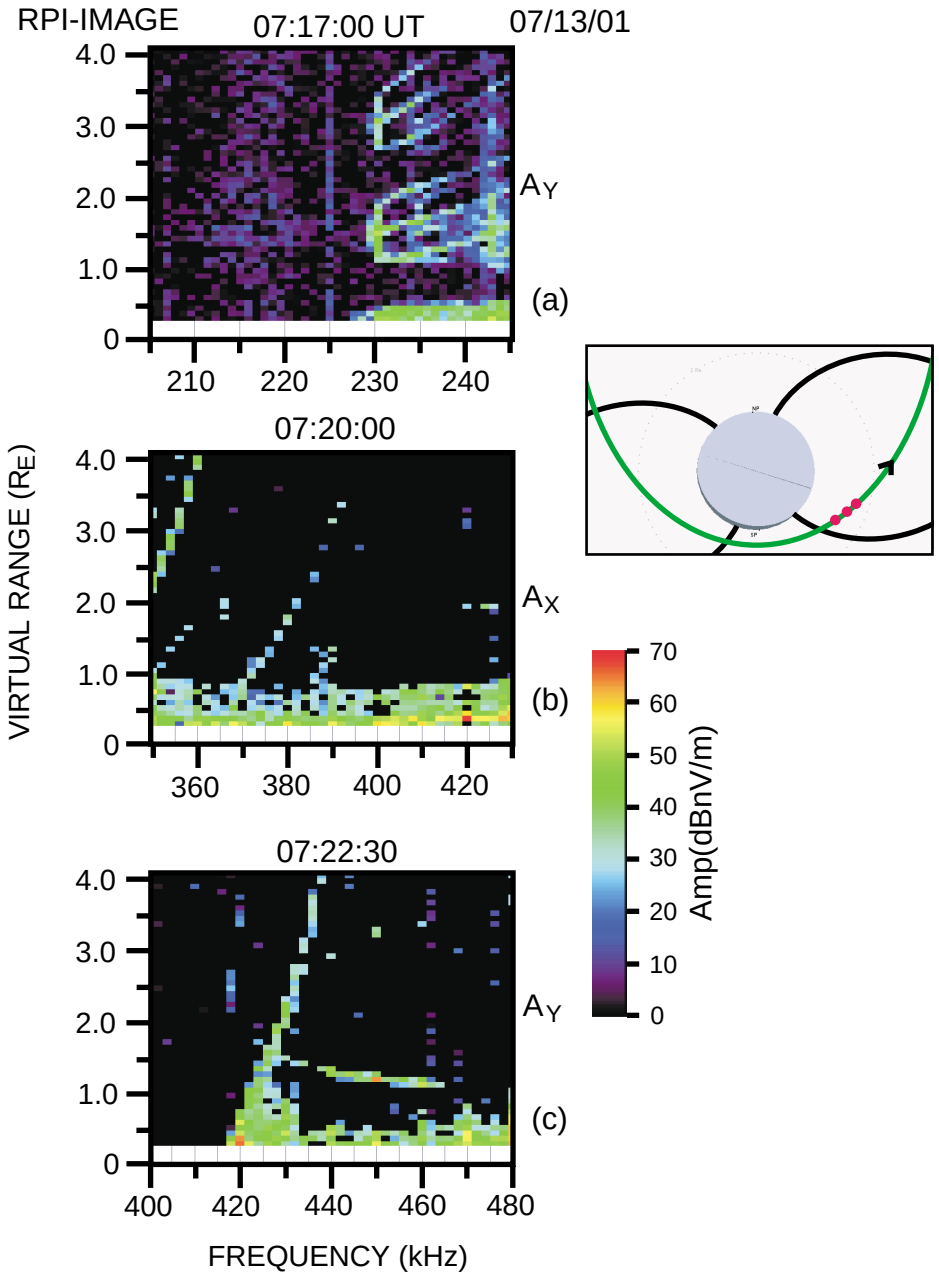

Figure 12. Examples from July 13, 2001 showing apparent changes in Z-mode echoes as IMAGE moved in the plasmasphere from a location below a Z-mode trough minimum (panel (a)) to a location above a minimum (panel (c)). Inset at the right shows the approximate locations of the three soundings.

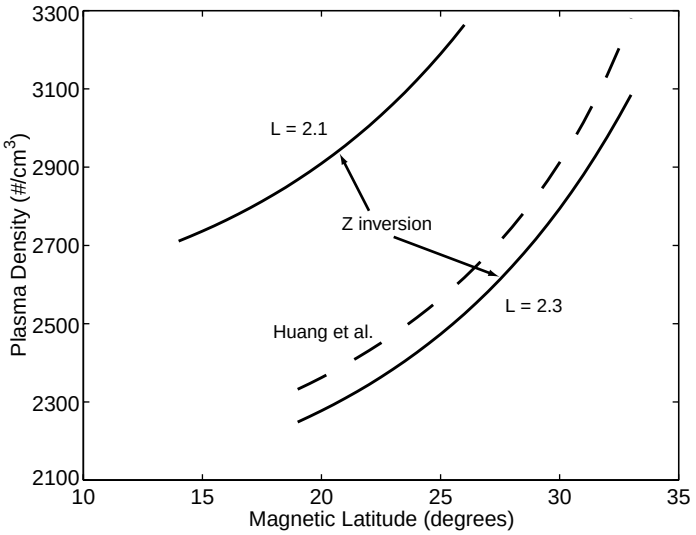

Figure 13. Plots of electron density versus magnetic latitude at two L values, inferred from the upward propagating Z-mode signals illustrated in Figures 8a and 8b. The dashed curve is for L = 2.3 within an empirical model developed by *Huang et al.*, [2003]. That model is based upon inversion of free-space echoes from RPI that propagated along multiple field aligned paths.

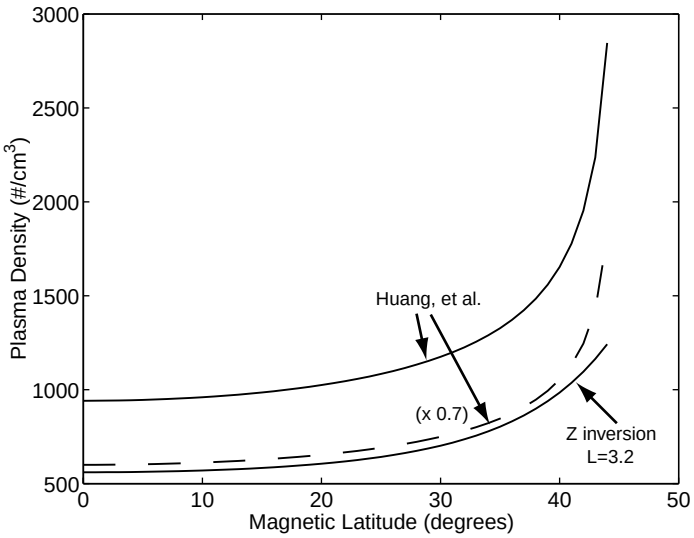

Figure 14. Plots of electron density versus magnetic latitude along field lines at L = 3.2. The lower solid curve is from the present work, while the upper solid curve is from the *Huang et al.* [2003] model noted in the previous figure caption, also applied to L = 3.2. The dashed curve is the result of scaling the *Huang et al.* result by a factor of 0.7.